J. Fluid Mech. (2000), *vol.* 410, *pp.* 285–322. Printed in the United Kingdom

Nonlinear magnetoconvection in the presence of strong oblique fields

By K. JULIEN[1], E. KNOBLOCH[2] AND S. M. TOBIAS[3]†

[1] Department of Applied Mathematics, University of Colorado, Boulder CO 80309, USA

[2] Department of Physics, University of California, Berkeley CA 94720, USA

[3] JILA, University of Colorado, Boulder CO 80309, USA

(Received 29 April 1999 and in revised form 22 December 1999)

Two-dimensional thermal convection in the presence of a strong oblique magnetic field is studied using an asymptotic expansion in inverse powers of the Chandrasekhar number. The linear stability problem reveals the existence of two distinct scales in the vertical structure of the critical eigenfunctions: a small length-scale whose vertical wavenumber k_z is comparable with the large horizontal wavenumber $k_\perp$ selected at onset, and a large-scale modulation which forms an envelope on the order of the layer depth d. The small-scale structure in the vertical results from magnetic alignment that forces fluid motions to be (nearly) parallel to the field lines. For convective transport in the vertical this constraint must be relaxed. This is achieved by molecular dissipation which allows weak upward (downward) motions of hot (cold) fluid elements across the field lines and results in a large-scale vertical modulation of the magnetic columns. Using the scaling suggested by the linear theory, strongly nonlinear steady and overstable solutions are constructed. These are characterized by large departures of the mean temperature profile from the conduction profile. For overstable rolls two modes of convection are uncovered. The first 'vertical field' mode is characterized by thin thermal boundary layers and a Nusselt number that increases rapidly with the applied Rayleigh number; this mode is typical of steady convection as well. The second or 'horizontal field' mode is present in overstable convection only and has broad thermal boundary layers and a Nusselt number that remains small and approximately independent of the Rayleigh number. At large Rayleigh numbers this regime is characterized by a piecewise linear temperature profile with a small isothermal core. The 'horizontal field' mode is favoured for substantial inclinations of the field and sufficiently small ohmic diffusivity. The transition between the two regimes is typically hysteretic and for fixed inclination and diffusivity may occur with increasing Rayleigh number. Similar but highly asymmetric states are obtained for depth-dependent ζ, where ζ is the ratio of ohmic to thermal diffusivity. These results are obtained from a nonlinear eigenvalue problem for the Nusselt number and mean temperature profile, and suggest a possible explanation for the sharp boundary between the umbra and penumbra in sunspots.

1. Introduction

The study of convection in an imposed magnetic field is motivated primarily by astrophysical applications and in particular by the observations of sunspots (Thomas

† Present address: Department of Applied Mathematical Studies, University of Leeds, Leeds LS2 9JT, UK.

& Weiss 1992). Motivated by this application several authors investigated the suppression of convection by strong magnetic fields. Within linear theory the details of this process are summarized by Chandrasekhar (1961). Veronis (1959) was the first to observe that nonlinear convection in a vertical magnetic field will be subcritical if the magnetic diffusivity is sufficiently small, and consequently that convection could be present even when no linear instability is predicted. This behaviour was studied by Weiss (1981*a*,*b*) in a series of numerical simulations; some studies of convection in an imposed horizontal field have also been carried out (Arter 1983; Hughes 1987; Cattaneo & Hughes 1988; Brownjohn *et al.* 1995). However, the magnetic field in sunspots is in general neither vertical nor horizontal, and this fact led Matthews *et al.* (1992) to undertake the first nonlinear investigation of convection in an oblique magnetic field. Although fully compressible this investigation was unable to reach the parameter values, both in terms of field strengths and Rayleigh number (a non-dimensional measure of the buoyancy force), characteristic of convection in sunspots. Even with today's state-of-the-art computers limitations on memory and computational speed place substantial restrictions on the accessible parameter range.

In the present paper we bring a new set of tools to bear on this problem. We exploit an asymptotic procedure first used in convection theory by Blennerhassett & Bassom (1994) and Bassom & Zhang (1994) to obtain strongly nonlinear solutions valid in the limit of large magnetic field strengths and substantially supercritical Rayleigh numbers. We use the term 'strongly nonlinear' to distinguish our work from weakly nonlinear theories in which the mean temperature profile is barely distorted by the motion. In contrast, the states we compute are characterized by strong, i.e. order one, distortions. This is accomplished by focusing on the small horizontal spatial scales and high-frequency oscillations predicted from the linear theory in the strong field limit, and leads to a reformulation of the problem as a nonlinear eigenvalue problem for the (time-averaged) Nusselt number (a non-dimensional measure of the vertical heat transport) and mean temperature profile as a function of the applied Rayleigh number. The scaling adopted follows that used by Julien, Knobloch & Tobias (1999*a*) for a vertically imposed magnetic field (see also Matthews 1999) but because of the tilt of the field the solution of the problem has more in common with the work of Julien & Knobloch (1998) on rapidly rotating convection on an f-plane.

In the present work we do not include the effects of compressibility although we do consider the effects of depth-dependent diffusivities as measured by $\zeta(z)$, the ratio of ohmic to thermal diffusivity. This effect is of particular importance in sunspots since $\zeta > 1$ favours steady overturning convection while $\zeta < 1$ favours overstable convection. Indeed the passage from $\zeta > 1$ to $\zeta < 1$ with increasing height has been linked to the formation of umbral dots (Weiss *et al.* 1990). We focus on two-dimensional structures in the form of tilted rolls, and discuss in detail the results for two orientations. In the so-called perpendicular case the roll axes are perpendicular to the plane containing the field and gravity; in the parallel case the roll axes are parallel to this plane (see figure 1). As is well known when the imposed field is horizontal these two configurations behave quite differently. This is because in the parallel case an interchange mode is available which avoids distortion of the field while allowing convection to proceed. In contrast, in the perpendicular case all motions distort the field and the onset of convection is delayed. When the field is inclined the distinction between these two configurations is less dramatic, since the magnetic field is sheared even in the parallel case.

In both cases we find two different 'modes' of overstable convection depending on parameters. The 'vertical field' mode is characterized by thin thermal boundary layers and a Nusselt number that increases rapidly with the applied Rayleigh number Ra

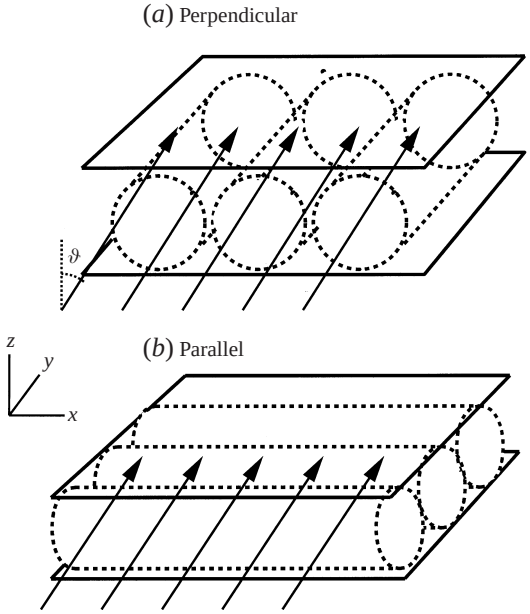

FIGURE 1. Sketch of (*a*) perpendicular rolls and (*b*) parallel rolls, as defined in the text. The imposed magnetic field makes an angle ϑ with respect to the vertical.

while the 'horizontal field' mode has broad thermal boundary layers and a Nusselt number that remains small and almost independent of *Ra*. At large *Ra* this regime is characterized by a piecewise linear temperature profile with a small isothermal core. The 'horizontal field' mode is favoured for substantial inclinations of the field and sufficiently small ohmic diffusivity. For typical inclinations and diffusivities a hysteretic transition from the 'vertical' to the 'horizontal' regime takes place as *Ra* increases. No comparable transition was found for steady convection.

We provide a physical explanation for these results, and compute self-consistently for each of these cases the associated horizontal mean flows, mean magnetic fields and heat fluxes, as a function of the field inclination. The results suggest a tentative explanation for the sharp transition between the umbra and penumbra in a sunspot: the increase in the tilt of the magnetic field with radial distance results in an abrupt change in the mode of convection, from a three-dimensional mode in the umbra to a two-dimensional mode consisting of parallel rolls in the penumbra. The resulting picture of sunspot convection has much in common with that recently put forward by Rucklidge, Schmidt & Weiss (1995) and is consistent with available observations.

This paper is organized as follows. In § 2 we introduce the governing equations. Section 3 contains a detailed description of the linear stability properties of the conduction state for finite but large values of the Chandrasekhar number (a non-dimensional measure of the magnetic field strength) and includes a comparison with the results obtained from an asymptotic expansion. Having validated the asymptotic expansion against the linear theory we proceed in § 4 to describe the asymptotic expansion that leads to a reduced description of the dynamics in the strong magnetic field limit; the equations that result are closely related to those obtained via the mean-field approximation (Van der Borght & Murphy 1973) but are asymptotically exact. In § 5 we specialize this description to two-dimensional rolls and derive a nonlinear eigenvalue problem describing their vertical structure. Section 6 contains

the results obtained by solving this problem in a variety of cases, focusing primarily on perpendicular and parallel rolls; these results are used in § 7 to compute self-consistently the mean horizontal flows, magnetic fields and heat fluxes associated with these solutions. The possible consequences for the structure of sunspots are discussed in § 8.

2. Governing equations

The dimensionless equations describing Boussinesq magnetoconvection in a plane horizontal layer are

$$\frac{1}{\sigma}\left(\frac{\partial}{\partial t}+\boldsymbol{v}\cdot\nabla\right)\boldsymbol{v}=-\nabla\pi+\zeta Q\boldsymbol{B}\cdot\nabla\boldsymbol{B}+RaT\hat{\boldsymbol{z}}+\nabla^2\boldsymbol{v}, \tag{2.1}$$

$$\left(\frac{\partial}{\partial t}+\boldsymbol{v}\cdot\nabla\right)T=\nabla^2T, \tag{2.2}$$

$$\left(\frac{\partial}{\partial t}+\boldsymbol{v}\cdot\nabla\right)\boldsymbol{B}=\boldsymbol{B}\cdot\nabla\boldsymbol{v}-\nabla\times(\zeta\nabla\times\boldsymbol{B}), \tag{2.3}$$

$$\nabla\cdot\boldsymbol{v}=0, \qquad \nabla\cdot\boldsymbol{B}=0, \tag{2.4}$$

where $\boldsymbol{v}=(u,v,w)$ is the velocity field in Cartesian coordinates (x,y,z) with z vertically upwards. The symbol T denotes the temperature, while π is the total (thermal and magnetic) pressure. The velocity field is written in the form $\boldsymbol{v}=\overline{\boldsymbol{U}}+\boldsymbol{u}$, where $\overline{\boldsymbol{U}}$ is the mean flow and $\boldsymbol{u}$ the convective flow. Likewise, the dimensionless magnetic field is assumed to be the superposition $\boldsymbol{B}=\hat{\boldsymbol{r}}+\overline{\boldsymbol{B}}+\boldsymbol{b}$ of an imposed oblique field of unit strength, a mean field $\overline{\boldsymbol{B}}$, and a three-dimensional field $\boldsymbol{b}$ both due to the presence of convection. The oblique field is denoted by $\hat{\boldsymbol{r}}=(\sin\vartheta,0,\cos\vartheta)$, where ϑ denotes the angle with respect to the vertical in the (x,z)-plane. The equations have been non-dimensionalized with respect to the thermal diffusion time in the vertical. The resulting dimensionless parameters

$$Q=\frac{B_0^2d^2}{\mu_0\rho\eta\nu}, \quad Ra=\frac{g\alpha\Delta Td^3}{\nu\kappa}, \quad \sigma=\frac{\nu}{\kappa}, \quad \zeta=\frac{\eta}{\kappa}, \tag{2.5}$$

are the Chandrasekhar, Rayleigh, and thermal and magnetic Prandtl numbers, respectively.† In the following ζ is allowed to vary with the depth while σ will be kept constant.

We employ a streamfunction formulation and write

$$\left.\begin{aligned}\boldsymbol{u}(x,y,z,t)&=\nabla\times\phi(x,y,z,t)\hat{\boldsymbol{z}}+\nabla\times\nabla\times\psi(x,y,z,t)\hat{\boldsymbol{z}},\\ \boldsymbol{b}(x,y,z,t)&=\nabla\times A(x,y,z,t)\hat{\boldsymbol{z}}+\nabla\times\nabla\times B(x,y,z,t)\hat{\boldsymbol{z}}.\end{aligned}\right\} \tag{2.6}$$

Thus

$$\boldsymbol{u}=\begin{pmatrix}\partial_y\phi & + & \partial_x\partial_z\psi\\ -\partial_x\phi & + & \partial_y\partial_z\psi\\ & - & \nabla_\perp^2\psi,\end{pmatrix}, \qquad \boldsymbol{b}=\begin{pmatrix}\partial_yA & + & \partial_x\partial_zB\\ -\partial_xA & + & \partial_y\partial_zB\\ & - & \nabla_\perp^2B,\end{pmatrix}, \tag{2.7}$$

† The non-dimensional parameters are defined in terms of the depth d of the layer, the imposed temperature difference ΔT between the bottom and top boundaries, and the magnitude B_0 of the imposed magnetic field. The remaining parameters are g (the local acceleration due to gravity), α (the coefficient of thermal expansion of the fluid), ν (the kinematic viscosity), κ (the thermal diffusivity), and η (the magnetic diffusivity). Finally, μ_0 is the magnetic permeability.

$$\boldsymbol{\omega} = \begin{pmatrix} \partial_x\partial_z\phi & - & \nabla^2\partial_y\psi \\ \partial_y\partial_z\phi & + & \nabla^2\partial_x\psi \\ & - & \nabla_\perp^2\phi \end{pmatrix}, \qquad \boldsymbol{j} = \begin{pmatrix} \partial_x\partial_z A & - & \nabla^2\partial_y B \\ \partial_y\partial_z A & + & \nabla^2\partial_x B \\ & - & \nabla_\perp^2 A \end{pmatrix}, \tag{2.8}$$

where $\boldsymbol{\omega} \equiv \nabla \times \boldsymbol{u}$ and $\boldsymbol{j} \equiv \nabla \times \boldsymbol{b}$ are, respectively, the vorticity and the current density. Partials with subscripts denote differentiation with respect to that variable, $\partial_x \equiv \partial/\partial x$, and $\nabla_\perp^2 \equiv \partial_{xx}^2 + \partial_{yy}^2$ is the horizontal Laplacian.

We find, *a posteriori*, that $\overline{\boldsymbol{U}}$ and $\overline{\boldsymbol{B}}$ are sufficiently small that they do not enter the leading-order dynamics, but may be determined self-consistently from the resulting Reynolds and magnetic stresses (see § 7). Consequently, we set for now $\overline{\boldsymbol{U}} = \overline{\boldsymbol{B}} = 0$; the four scalar fields ϕ, ψ, A, B and the temperature T then satisfy the equations

$$\frac{1}{\sigma}(\partial_t\nabla_\perp^2\phi + N_\phi) = \zeta Q(\hat{\boldsymbol{r}}\cdot\nabla\nabla_\perp^2 A + M_\phi) + \nabla^2\nabla_\perp^2\phi, \tag{2.9}$$

$$\frac{1}{\sigma}(\partial_t\nabla^2\nabla_\perp^2\psi + N_\psi) = -Ra\nabla_\perp^2 T + \zeta Q(\hat{\boldsymbol{r}}\cdot\nabla\nabla^2\nabla_\perp^2 B + M_\psi) + \nabla^4\nabla_\perp^2\psi, \tag{2.10}$$

$$\partial_t T + N_T = \nabla^2 T, \tag{2.11}$$

$$\partial_t\nabla_\perp^2 A + M_A = \hat{\boldsymbol{r}}\cdot\nabla\nabla_\perp^2\phi + \zeta\nabla^2\nabla_\perp^2 A + (\partial_z\zeta)\partial_z\nabla_\perp^2 A, \tag{2.12}$$

$$\partial_t\nabla_\perp^2 B + M_B = (\hat{\boldsymbol{r}}\cdot\nabla)\nabla_\perp^2\psi + \zeta\nabla^2\nabla_\perp^2 B. \tag{2.13}$$

The nonlinear terms N_ϕ, M_ϕ, N_ψ, N_T, M_ψ, M_A and M_B are written down in full in the Appendix.

These equations are solved for a fluid confined between impenetrable boundaries at fixed temperatures,

$$T|_{z=0} = 1, \qquad T|_{z=1} = 0, \tag{2.14}$$

that are either stress-free or no-slip. The simplest magnetic boundary conditions, employed by Matthews *et al.* (1992), require that the field be tilted by the same angle ϑ to the vertical everywhere on the top and bottom boundaries. However, in the following we find that the detailed nature of the boundary conditions becomes unimportant in the large-Q limit; the solutions for different magnetic or velocity boundary conditions differ in thin passive boundary layers at top and bottom only. Periodic boundary conditions in the horizontal are used throughout.

3. Linear theory

Throughout this paper we shall distinguish two main types of configuration: convection in which the roll axes are perpendicular to the (x, z)-plane containing gravity and the magnetic field, and the parallel case in which they lie in the planes $y = \text{const}$ (see figure 1). We describe the roll orientation in terms of the wave vector $\boldsymbol{k}_0 = (k_{0x}, k_{0y}, k_{0z})$ of the rolls, where $k_{0x} = k_{0\perp}\cos\chi$, $k_{0y} = k_{0\perp}\sin\chi$, and $k_{0\perp}$ denotes the horizontal wavenumber. Thus the perpendicular case corresponds to $\chi = 0$ while the parallel case corresponds to $\chi = \pi/2$; intermediate orientations correspond to $0 < \chi < \pi/2$. The vertical component k_{0z} is necessary in order to describe rolls aligned with the imposed magnetic field (see below).

In this section we briefly summarize the linear stability properties of the conduction solution $\boldsymbol{v} = 0$, $T = 1 - z$, $\boldsymbol{B} = \hat{\boldsymbol{r}}$ in the two cases $\chi = 0$, $\chi = \pi/2$ obtained with stress-free boundaries and fixed field inclination. Figure 2(a, b) shows the critical Rayleigh number Ra_c and the corresponding wavenumber k_c (i.e. the value of $k_{0\perp}$

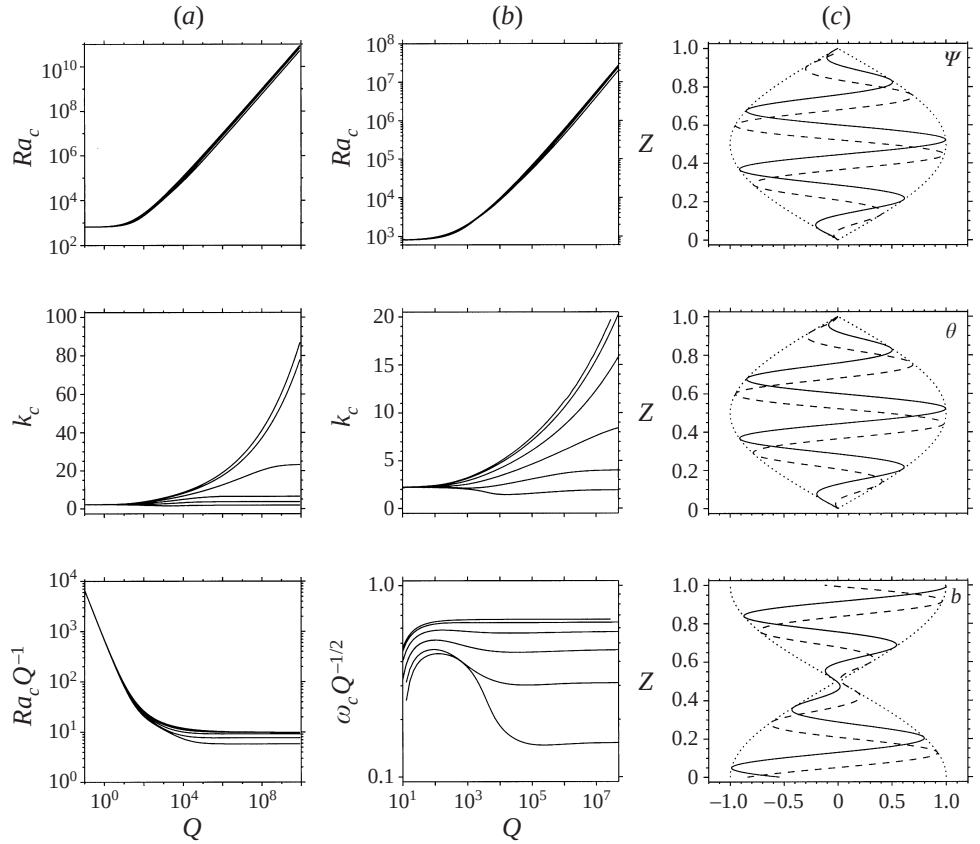

FIGURE 2. The critical Rayleigh number Ra_c and wavenumber k_c for onset of (*a*) steady, and (*b*) oscillatory perpendicular rolls ($\chi = 0$) as functions of Q for $\vartheta = 0°$, 15°, 30°, 45°, 60°, 75° and $\zeta = 0.1$. The bottom panels show the approach of, respectively, $Ra_c(Q)$ and $\omega_c(Q)$ to their asymptotic values at large Q. (*c*) The exact vertical eigenfunction for steady onset when $\chi = 0$, $\vartheta = \pi/12$ and $Q = 6.8261 \times 10^9$; for these parameters $Ra_c^{(s)} = 6.7485 \times 10^{10}$, $k_c^{(s)} = 74.6398$. The eigenfunction is complex with solid (dashed) lines denoting its real (imaginary) parts, and reveals the presence of two scales in the vertical. The dotted lines show the slowly varying envelope.

that minimizes Ra) as a function of Q for steady and oscillatory convection for several different values of the tilt angle ϑ when $\chi = 0$. As expected, the critical Rayleigh number increases rapidly with increasing Q, i.e. the magnetic field has a stabilizing effect. This effect depends only weakly on the tilt angle but decreases as this angle increases. The third panel in figure 2(*a*) shows the approach of $Ra_c(Q)$ to its asymptotic behaviour, and confirms that in this regime $Ra_c = O(Q)$ for the tilt angles considered. This is so also for oscillatory onset. Somewhat unexpected, however, is the behaviour of the associated k_c for large Q. One expects that $k_c = O(Q^{1/6})$ but this behaviour is found only for tilt angles that are small enough; for tilt angles exceeding approximately 30° an $O(1)$ wavenumber is selected instead. These results reflect the dominant component of the field: for steady convection in an imposed vertical field, $k_c \sim (\frac{1}{2}\pi^4 Q)^{1/6}$ while for an imposed horizontal field, $k_c \sim \pi^{3/2} Q^{-1/4}$. In both cases $Ra_c \sim \pi^2 Q$. These two types of behaviour indicate that as the tilt angle increases the system undergoes a transition in which its behaviour changes from one in which the vertical field dominates to one in which the horizontal field

dominates. We shall see that such a transition occurs in the nonlinear regime as well. In contrast, for parallel rolls $k_c \sim (\frac{1}{2}\pi^4 Q\cos^2\vartheta)^{1/6}$, $Ra_c \sim \pi^2\cos^2\vartheta Q$, provided that $Q\cos^2\vartheta \gg 1$, and the transition to the horizontal field behaviour occurs only for tilt angles $\vartheta = \pi/2 - O(Q^{-1/2})$. Thus in the parallel case large wavenumbers are selected for almost all tilt angles, but this is so only in a limited range of tilt angles in the perpendicular case. In fact the parallel case is special only when $\vartheta \sim \pi/2$, i.e. when the imposed field is essentially horizontal. In this case the magnetic field has no effect on the onset of convection and the selected wavenumber is therefore $O(1)$. In the limit of large Q the above results hold for no-slip boundaries as well.

In the following we find, following Julien *et al.* (1999*a*), that for $O(1)$ tilt angles an analysis with $O(Q^{1/4})$ horizontal wavenumbers describes correctly not only the linear and nonlinear properties of solutions with these wavenumbers but also those with the $O(Q^{1/6})$ wavenumbers selected by linear theory as described above. In particular, the zero wavenumber limit of the results given below yields the correct Rayleigh number and frequency that results from using an $O(Q^{1/6})$ scaling. In addition the analysis with $O(Q^{1/4})$ wavenumbers captures the transition from overstable convection preferred at small ζ to steady overturning convection preferred for $\zeta > 1$. As a result we can determine fully nonlinear steady states from the equations describing oscillatory convection by simply setting the oscillation frequency equal to zero, while retaining the wavenumber dependence of the solutions. This is in contrast to the $O(Q^{1/6})$ scaling which leads to distinct problems for steady and oscillatory convection, and yields results that are entirely wavenumber independent (Matthews 1999). These properties are the consequence of the very flat neutral stability curve in this wavenumber range.

In either case the dominant balance in the large-Q limit reflects the tendency of the inclined magnetic field to force the perturbation wavenumber $\boldsymbol{k}_0$ to be perpendicular to it: $\hat{\boldsymbol{r}}\cdot\boldsymbol{k}_0 = 0$. As a result unless $\chi = \pi/2$ the fast horizontal variation due to the small horizontal wavenumber translates into rapid variation in the vertical ($k_{0z} = -k_{0x}\tan\vartheta$; see figure 2*c*). Physically, this is the result of the alignment of the narrow convection rolls selected at onset with the imposed tilted field. This fact motivates the introduction of a two-scale approach to describe the vertical structure of the resulting convection, as discussed in the next section. In the large-Q limit the linear stability results for $O(Q^{1/4})$ wavenumbers become independent of the nature of the velocity and magnetic boundary conditions at the top and bottom of the layer and can therefore be determined analytically:

$$Ra^{(s)} = \left(1+\cos^2\chi\tan^2\vartheta\right)[\pi^2\cos^2\vartheta Q + (1+\cos^2\chi\tan^2\vartheta)^2 k_{0\perp}^4], \tag{3.1}$$

where $k_0^2 = k_{0\perp}^2(1+\cos^2\chi\tan^2\vartheta)$. The minimum occurs at $k_{0\perp} = 0$:

$$Ra_c^{(s)} = \left(1+\cos^2\chi\tan^2\vartheta\right)\pi^2\cos^2\vartheta Q. \tag{3.2}$$

This equation predicts that for $\chi = 0$ Ra_c is independent of ϑ, in good agreement with the results of figure 2. Likewise, for $\zeta < 1$, the onset of overstable oscillations occurs at

$$Ra^{(o)} = \left(1+\cos^2\chi\tan^2\vartheta\right)\left[\frac{\sigma+\zeta}{\sigma(1+\sigma)}\right] \times[\pi^2\cos^2\vartheta\sigma\zeta Q + (1+\sigma)(1+\zeta)(1+\cos^2\chi\tan^2\vartheta)^2 k_{0\perp}^4], \tag{3.3}$$

$$\omega^{(o)2} = \frac{\zeta}{(1+\sigma)}[(1-\zeta)\pi^2\cos^2\vartheta\sigma Q - \zeta(1+\sigma)(1+\cos^2\chi\tan^2\vartheta)^2 k_{0\perp}^4]. \tag{3.4}$$

Again, the minimum occurs at $k_{0\perp} = 0$:

$$Ra_c^{(o)} = \left(1 + \cos^2\chi \tan^2\vartheta\right)\left(\frac{\sigma+\zeta}{1+\sigma}\right)\pi^2\cos^2\vartheta\zeta Q, \qquad \omega_c^{(o)2} = \left(\frac{1-\zeta}{1+\sigma}\right)\pi^2\cos^2\vartheta\sigma\zeta Q \tag{3.5}$$

and is independent of ϑ when $\chi = 0$. Furthermore, $Ra_c^{(o)} < Ra_c^{(s)}$. In these expressions the wavenumber $k_{0\perp}$ is the physical horizontal wavenumber, i.e. $k_{0\perp} = O(Q^{1/4})$. The selection of $k_{0\perp} = 0$ is thus a reflection of the selection of a smaller wavenumber, namely $k_{0\perp} = O(Q^{1/6})$. However, the $Q^{1/4}$ scaling determines correctly the resulting minimum Rayleigh numbers and frequency. Moreover, as pointed out by Chandrasekhar (1961), the $O(Q^{1/4})$ scaling also captures the transition from steady to oscillatory convection. This transition takes place when $\omega_c^{(o)} = 0$, i.e. at

$$Ra_{TB} = \left(1 + \cos^2\chi \tan^2\vartheta\right)\left[\frac{\sigma+\zeta}{\zeta(1+\sigma)}\right]\pi^2\cos^2\vartheta Q, \tag{3.6}$$

$$k_{\perp TB} = \left[\frac{\pi\cos\vartheta}{(1+\cos^2\chi\tan^2\vartheta)}\right]^{1/2}\left[\frac{\sigma(1-\zeta)}{\zeta(1+\sigma)}\right]^{1/4} Q^{1/4}, \tag{3.7}$$

and defines the Takens–Bogdanov (TB) point. Consequently the $O(Q^{1/4})$ scaling describes correctly not only the vicinity of the Takens–Bogdanov point but also the behaviour for onset wavenumbers far from this point, i.e. it allows us to retain the full wavenumber dependence of the problem.

We do not give a detailed derivation of these results since these follow immediately from those obtained in the following section. For future reference we note that when $\vartheta = 0$ all χ dependence necessarily drops out. However, in contrast to the moderate-Q results of Matthews *et al.* (1992) $Ra_c(\chi = \pi/2) < Ra_c(\chi = 0)$ for all $\vartheta \neq 0$ and hence away from the Takens–Bogdanov point the large-Q linear theory suggests that parallel rolls are always selected at onset. In § 8 we identify a plausible mechanism that selects between the two roll orientations in the fully nonlinear regime.

4. The reduced equations

For large values of the Chandrasekhar number Q simplified equations describing the nonlinear problem can be obtained using the scaling (cf. Julien *et al.* 1999*a*)

$$(x, y, z) = Q^{-1/4}(x', y', z'), \qquad t = Q^{-1/2}t', \tag{4.1}$$

suggested in the preceding section. With this scaling we focus on small horizontal and vertical scales (and high-frequency oscillations in the case of overstable convection). As in the related problem of convection on a rapidly rotating f-plane (Julien & Knobloch 1998) the linear eigenfunction must also vary on an $O(1)$ vertical scale which we denote by Z (see figure 2*c*). Consequently we set

$$\partial_x, \partial_y = Q^{1/4}(\partial_{x'}, \partial_{y'}), \quad \partial_z = Q^{1/4}(\partial_{z'} + Q^{-1/4}\mathrm{D}), \quad \partial_t = Q^{1/2}\partial_{t'}, \tag{4.2}$$

where $\mathrm{D} \equiv \partial_Z$. The resulting expansion reflects the tendency towards small-scale motion aligned with the inclined magnetic field. We focus on $O(Q)$ Rayleigh numbers, i.e. we also write

$$Ra = QRa', \tag{4.3}$$

but in contrast to Proctor (1986) do not scale the thermal and magnetic Prandtl numbers, which are assumed to remain of order one. In this regime the convective

motions do not distort the field substantially and the dominant nonlinear effect arises from the distortion of the mean temperature profile. Finally, the fluid variables are scaled according to

$$\phi = \phi'(x', y', z', Z, t') + O(Q^{-1/4}), \tag{4.4}$$

$$\psi = Q^{-1/4}\psi'(x', y', z', Z, t') + O(Q^{-1/2}), \tag{4.5}$$

$$A = Q^{-1/2}A'(x', y', z', Z, t') + O(Q^{-3/4}), \tag{4.6}$$

$$B = Q^{-3/4}B'(x', y', z', Z, t') + O(Q^{-1}), \tag{4.7}$$

$$T = \theta_0(Z) + Q^{-1/4}\theta'(x', y', z', Z, t') + O(Q^{-1/2}). \tag{4.8}$$

These scalings imply that the velocity and magnetic field perturbations are (approximately) isotropic with $\boldsymbol{u} \approx O(Q^{1/4})$ and $\boldsymbol{b} \approx O(Q^{-1/4})$ although, as shown below, the toroidal fields in fact decouple from the poloidal ones. Such a decoupling is to be expected in a weakly nonlinear description but its occurrence here in a fully nonlinear theory is not *a priori* obvious.

We next introduce the notation

$$\nabla = \nabla_0 + Q^{-1/4}\mathrm{D}\hat{\boldsymbol{z}}, \quad \nabla_0 = (\partial_{x'}, \partial_{y'}, \partial_{z'}), \quad \nabla_{0\perp} = (\partial_{x'}, \partial_{y'}, 0), \tag{4.9}$$

$$\nabla^2 = (\nabla_0^2 + 2Q^{-1/4}\partial_{z'}\mathrm{D} + Q^{-1/2}\mathrm{D}^2), \quad \nabla_0^2 = \partial^2_{x'x'} + \partial^2_{y'y'} + \partial^2_{z'z'}. \tag{4.10}$$

The equations describing the departure from the conduction state now become (dropping primes)

$$-\zeta\hat{\boldsymbol{r}}\cdot\nabla_0\nabla^2_{0\perp}A = Q^{-1/4}[\zeta(\hat{r}_z\mathrm{D}\nabla^2_{0\perp}A + M_\phi) + \nabla_0^2\nabla^2_{0\perp}\phi - \frac{1}{\sigma}(\partial_t\nabla^2_{0\perp}\phi + N_\phi)] + O(Q^{-1/2}), \tag{4.11}$$

$$-\zeta\hat{\boldsymbol{r}}\cdot\nabla_0\nabla_0^2\nabla^2_{0\perp}B = Q^{-1/4}\left[\zeta(\hat{r}_z\mathrm{D}\nabla_0^2\nabla^2_{0\perp}B + M_\psi) + \nabla_0^4\nabla^2_{0\perp}\psi - \frac{1}{\sigma}(\partial_t\nabla_0^2\nabla^2_{0\perp}\psi + N_\psi) - Ra\nabla^2_{0\perp}\theta\right] + O(Q^{-1/2}), \tag{4.12}$$

$$-\hat{\boldsymbol{r}}\cdot\nabla_0\nabla^2_{0\perp}\phi = Q^{-1/4}(\hat{r}_z\mathrm{D}\nabla^2_{0\perp}\phi + \zeta\nabla_0^2\nabla^2_{0\perp}A - \partial_t\nabla^2_{0\perp}A - M_A) + O(Q^{-1/2}), \tag{4.13}$$

$$-\hat{\boldsymbol{r}}\cdot\nabla_0\nabla^2_{0\perp}\psi = Q^{-1/4}(\hat{r}_z\mathrm{D}\nabla^2_{0\perp}\psi + \zeta\nabla_0^2\nabla^2_{0\perp}B - \partial_t\nabla^2_{0\perp}B - M_B) + O(Q^{-1/2}), \tag{4.14}$$

with the temperature equation given by

$$\partial_t T + Q^{-1/2}N_T = \nabla_0^2 T. \tag{4.15}$$

These equations are solved by an asymptotic expansion of the form

$$\boldsymbol{\Psi} = \boldsymbol{\Psi}_1 + Q^{-1/4}\boldsymbol{\Psi}_2 + Q^{-1/2}\boldsymbol{\Psi}_3 + \cdots, \tag{4.16}$$

where $\boldsymbol{\Psi} \equiv (\phi, \psi, \theta, A, B)^T$. At $O(Q^0)$ one obtains

$$\hat{\boldsymbol{r}}\cdot\nabla_0\nabla^2_{0\perp}A_1 = 0, \quad \hat{\boldsymbol{r}}\cdot\nabla_0\nabla_0^2\nabla^2_{0\perp}B_1 = 0, \quad \hat{\boldsymbol{r}}\cdot\nabla_0\nabla^2_{0\perp}\phi_1 = 0, \quad \hat{\boldsymbol{r}}\cdot\nabla_0\nabla^2_{0\perp}\psi_1 = 0. \tag{4.17}$$

Thus on small scales all perturbations align with the imposed magnetic field. Solutions of this type take the form

$$\boldsymbol{\Psi}_1(\boldsymbol{x}, Z, t) = \int \hat{\boldsymbol{\Psi}}_1(\boldsymbol{k}_0, Z, t)\mathrm{e}^{\mathrm{i}\boldsymbol{k}_0\cdot\boldsymbol{x}}\mathrm{d}\boldsymbol{k}_0 + \text{ c.c.}, \tag{4.18}$$

where $\boldsymbol{k}_0 \cdot \hat{\boldsymbol{r}} = 0$. Since $\hat{\boldsymbol{r}} = (\sin\vartheta, 0, \cos\vartheta)$ and $(k_{0x}, k_{0y}) = k_{0\perp}(\cos\chi, \sin\chi)$ it follows that $k_{0z} = -k_{0x}\tan\vartheta = -k_{0\perp}\cos\chi\tan\vartheta$.

The solvability condition at $O(Q^{-1/4})$ yields evolution equations for the amplitudes $\hat{\boldsymbol{\Psi}}_1(\boldsymbol{k}_0, Z, t)$:

$$\frac{1}{\sigma}\left(\partial_t\hat{\phi}_1 - \frac{1}{k_{0\perp}^2}PN_\phi(\boldsymbol{\Psi}_1)\right) = \zeta\left(\hat{r}_z\mathrm{D}\hat{A}_1 - \frac{1}{k_{0\perp}^2}PM_\phi(\boldsymbol{\Psi}_1)\right) - k_0^2\hat{\phi}_1, \tag{4.19}$$

$$\frac{1}{\sigma}\left(\partial_t\hat{\psi}_1 + \frac{1}{k_0^2k_{0\perp}^2}PN_\psi(\boldsymbol{\Psi}_1)\right) = \frac{Ra}{k_0^2}\hat{\theta}_1 + \zeta\left(\hat{r}_z\mathrm{D}\hat{B}_1 + \frac{1}{k_0^2k_{0\perp}^2}PM_\psi(\boldsymbol{\Psi}_1)\right) - k_0^2\hat{\psi}_1, \tag{4.20}$$

$$\partial_t\hat{A}_1 - \frac{1}{k_{0\perp}^2}PM_A(\boldsymbol{\Psi}_1) = \hat{r}_z\mathrm{D}\hat{\phi}_1 - \zeta k_0^2\hat{A}_1, \tag{4.21}$$

$$\partial_t\hat{B}_1 - \frac{1}{k_{0\perp}^2}PM_B(\boldsymbol{\Psi}_1) = \hat{r}_z\mathrm{D}\hat{\psi}_1 - \zeta k_0^2\hat{B}_1, \tag{4.22}$$

where P is a projection operator that filters out the fast spatial variation defined by:

$$Pf(\boldsymbol{\Psi}_1) \equiv \frac{1}{(2\pi)^3}\int \mathrm{e}^{-\mathrm{i}\boldsymbol{k}_0\cdot\boldsymbol{x}}f(\boldsymbol{\Psi}_1)\,\mathrm{d}\boldsymbol{x}. \tag{4.23}$$

The projection P is thus equivalent to averaging over the fast spatial scales and plays much the same role as the temporal averaging operator in the work of Babin, Mahalov & Nicolaenko (1994) on rapidly rotating turbulence.

The temperature equation yields the following equations at $O(Q^{1/4})$ and $O(Q^0)$, respectively:

$$\partial_t\theta_1 - \mathrm{J}[\phi_1,\theta_1] + (\nabla_{0\perp}\partial_z\psi_1\cdot\nabla_{0\perp}\theta_1 - \nabla_{0\perp}^2\psi_1\partial_z\theta_1) - \nabla_{0\perp}^2\psi_1\mathrm{D}\theta_0 = \nabla_0^2\theta_1, \tag{4.24}$$

$$\begin{aligned}\partial_t\theta_2 &- \mathrm{J}[\phi_1,\theta_2] - J[\phi_2,\theta_1] + (\nabla_{0\perp}\partial_z\psi_1\cdot\nabla_{0\perp}\theta_2 - \nabla_{0\perp}^2\psi_1\partial_z\theta_2)\\ &+ (\nabla_{0\perp}\partial_z\psi_2\cdot\nabla_{0\perp}\theta_1 - \nabla_{0\perp}^2\psi_2\partial_z\theta_1) + (\nabla_{0\perp}\mathrm{D}\psi_1\cdot\nabla_{0\perp}\theta_1 - \nabla_{0\perp}^2\psi_1\mathrm{D}\theta_1)\\ &- \nabla_{0\perp}^2\psi_2\mathrm{D}\theta_0 = \nabla_0^2\theta_2 + 2\partial_z\mathrm{D}\theta_1 + \mathrm{D}^2\theta_0.\end{aligned} \tag{4.25}$$

Equation (4.24) can be solved for θ_1. Once this is done the solvability condition for the mean part of θ_2 yields

$$\mathrm{D}^2\theta_0 + \mathrm{D}(\overline{\nabla_\perp^2\psi_1\theta_1}) = 0, \tag{4.26}$$

which can be integrated once, obtaining

$$\mathrm{D}\theta_0 + \overline{\nabla_\perp^2\psi_1\theta_1} = -K. \tag{4.27}$$

For steady patterns the constant K is identified with the Nusselt number; for oscillatory patterns we extend the meaning of the overbar to indicate an average over time as well. For such patterns K represents the time-averaged Nusselt number.

Since the complications arising from the presence of the projection P are absent in the linear problem we can use the linearized equations (4.19)–(4.24) to solve the linear stability in the limit of large Q. We then recover the asymptotic results reported in § 3.

5. Tilted rolls

Equations (4.19)–(4.22) and (4.24), (4.27) constitute a closed set of equations for the evolution of the vertical profile of the different fields. The simplest case of such

evolution is offered by (tilted) two-dimensional roll solutions of the form

$$\Psi_1 = \Psi_L(Z)\exp(\mathrm{i}\omega t + \mathrm{i}\boldsymbol{k}_0\cdot x) + \Psi_R(Z)\exp(\mathrm{i}\omega t - \mathrm{i}\boldsymbol{k}_0\cdot x) + \text{c.c.}, \tag{5.1}$$

where $\Psi_1 = (\phi_1, \psi_1, \theta_1, A_1, B_1)$. For these solutions none of the nonlinear terms $N_\phi, M_\phi, N_\psi, M_\psi, M_A, M_B$ contributes to the leading-order solvability conditions which reduce to a simple set of linear equations:

$$\left.\begin{aligned} &(\mathrm{i}\omega + \zeta k_0^2)A_{(L,R)} = \hat{r}_z \mathrm{D}\phi_{(L,R)}, \quad (i\omega + \zeta k_0^2)B_{(L,R)} = \hat{r}_z \mathrm{D}\psi_{(L,R)}, \\ &\left(\frac{\mathrm{i}\omega}{\sigma} + k_0^2\right)\phi_{(L,R)} = \zeta \hat{r}_z \mathrm{D}A_{(L,R)}, \quad \left(\frac{\mathrm{i}\omega}{\sigma} + k_0^2\right)k_0^2\psi_{(L,R)} = Ra\theta_{(L,R)} + \zeta k_0^2 \hat{r}_z \mathrm{D}B_{(L,R)}. \end{aligned}\right\} \tag{5.2}$$

Moreover,

$$(\mathrm{i}\omega + k_0^2)\theta_{(L,R)} = -k_{0\perp}^2 \psi_{(L,R)}\,\mathrm{D}\theta_0. \tag{5.3}$$

These equations have a circle of solutions of the form $\Xi_L = c\Xi_R$, where $\Xi_{L,R}(Z) = (\Phi_{L,R}(Z), \Psi_{L,R}(Z), \Theta_{L,R}(Z), A_{L,R}(Z), B_{L,R}(Z))$ and c is an arbitrary complex constant. The particular cases $c = 0$ and $c = \exp \mathrm{i}\varphi$, where φ is a phase, correspond respectively to travelling and standing waves. All these solutions satisfy the same equations, as can be seen by introducing the transformation

$$\Xi_L = \frac{\Xi}{\sqrt{1+|c|^2}}, \qquad \Xi_R = \frac{c\Xi}{\sqrt{1+|c|^2}}, \tag{5.4}$$

where $\Xi(Z) = (\Phi(Z), \Psi(Z), \Theta(Z), A(Z), B(Z))$. From equation (4.27) we now obtain

$$\mathrm{D}\theta_0\left[1 + \frac{2k_0^2 k_{0\perp}^4}{\omega^2 + k_0^4}|\Psi|^2\right] = -K, \tag{5.5}$$

with K given by the requirement that $\theta_0(0) = 1$, $\theta_0(1) = 0$:

$$K = \left[\int_0^1 \frac{\omega^2 + k_0^4}{\omega^2 + k_0^4 + 2k_0^2 k_{0\perp}^4 |\Psi|^2}\mathrm{d}Z\right]^{-1}. \tag{5.6}$$

From the ψ, θ and B equations we now obtain the nonlinear eigenvalue problem

$$\mathrm{D}^2\Psi - \frac{(\mathrm{D}\zeta)k_0^2}{\mathrm{i}\omega + \zeta k_0^2}\mathrm{D}\Psi - \frac{1}{\hat{r}_z^2\zeta}\left(\frac{\mathrm{i}\omega}{\sigma} + k_0^2\right)(\mathrm{i}\omega + \zeta k_0^2)\Psi + \frac{RaK}{\hat{r}_z^2\zeta}\frac{(\mathrm{i}\omega + \zeta k_0^2)(-\mathrm{i}\omega + k_0^2)}{\omega^2 + k_0^4 + 2k_0^2 k_{0\perp}^4|\Psi|^2}\frac{k_{0\perp}^2}{k_0^2}\Psi = 0. \tag{5.7}$$

The solutions of this problem depend on the prescribed function $\zeta(z)$ as well as the parameters Ra, k_0, $k_{0\perp}$ and σ. In the case where ζ is constant equation (5.7) reduces to

$$\mathrm{D}^2\Psi - \frac{1}{\hat{r}_z^2\zeta}\left(\frac{\mathrm{i}\omega}{\sigma} + k_0^2\right)(\mathrm{i}\omega + \zeta k_0^2)\Psi + \frac{RaK}{\hat{r}_z^2\zeta}\frac{(\mathrm{i}\omega + \zeta k_0^2)(-\mathrm{i}\omega + k_0^2)}{\omega^2 + k_0^4 + 2k_0^2 k_{0\perp}^4|\Psi|^2}\frac{k_{0\perp}^2}{k_0^2}\Psi = 0. \tag{5.8}$$

In these equations $k_0^2 = k_{0\perp}^2(1 + \cos^2\chi\tan^2\vartheta)$. Note that when ζ is constant steady solutions ($\omega = 0$) are independent of both σ and ζ. The latter is not generally true and for finite Q the steady solutions do depend on ζ.

In contrast the Φ and A equations yield the linear eigenvalue problem:

$$\mathrm{D}^2\Phi - \frac{(\mathrm{D}\zeta)k_0^2}{\mathrm{i}\omega + \zeta k_0^2}\mathrm{D}\Phi = \frac{1}{\hat{r}_z^2\zeta}\left(\frac{\mathrm{i}\omega}{\sigma} + k_0^2\right)(\mathrm{i}\omega + \zeta k_0^2)\Phi. \tag{5.9}$$

Since ω is already known from equation (5.7) this problem typically has only the trivial solution $\Phi \equiv 0$, implying $A \equiv 0$. Hence no toroidal components are present.

6. Results

Equations (5.7), (5.8) are to be solved subject to the boundary conditions

$$\Psi(0) = \Psi(1) = 0, \tag{6.1}$$

imposing impermeability of the boundaries. As already indicated these boundary conditions are the appropriate ones for solution in the bulk, outside of thin (and passive) boundary layers required by specific velocity and magnetic field boundary conditions. We solve this problem on a discretized one-dimensional mesh using an iterative Newton–Raphson–Kantorovich scheme (Henrici 1962; Cash & Singhal 1982) with $O(10^{-10})$ accuracy in the L_2 norm of $\Psi(Z)$ and the corresponding eigenvalues. The solution determines K and ω for a two-parameter family of solutions depending on the complex parameter c, whose vertical profile is given in terms of the eigenfunction $\Psi(Z)$ by (5.4).

In the following we present detailed results for different tilt angles ϑ in the perpendicular ($\chi = 0$) and parallel ($\chi = \pi/2$) cases. When the imposed field is vertical ($\vartheta = 0$) these two situations are indistinguishable. However, as mentioned in the introduction, in the extreme case of a horizontal field ($\vartheta = \pi/2$) they behave in a fundamentally different way. We begin with the case of constant ζ, with the effects of a depth-dependent ζ described in § 6.4.

6.1. *Perpendicular rolls:* $\chi = 0$

We first discuss our results for the perpendicular case $\chi = 0$. We set the horizontal wavenumber $k_{0\perp} = 1.0$ and Prandtl number $\sigma = 1.1$ and focus on the changes in the solutions as the tilt angle ϑ and the magnetic diffusivity ζ are changed. Effects of changing the wavenumber are discussed in § 6.5.

When ζ is sufficiently small the linear theory in § 3 shows that oscillatory solutions are the first to set in; thus oscillatory convection transports heat more efficiently (at least near onset) than steady convection. Consequently we set $\zeta = 0.1$ and investigate the changes as the tilt angle ϑ is increased from zero. Figure 3(*a*) shows the Rayleigh number dependence of the (time-averaged) Nusselt number K for both steady and oscillatory convection for a relatively small tilt angle, $\vartheta = \pi/18$. The frequency of the oscillations is shown in figure 3(*b*). As in the vertical case discussed by Julien *et al.* (1999*a*) the Nusselt number is a monotonically increasing function of Ra and the frequency tends to a constant value in the limit of large Ra, indicating that the oscillations are of magnetic origin.

In figure 4 we show $|\Psi(Z)|$ (figure 4*a*) and the corresponding mean temperature $\theta_0(Z)$ (figure 4*b*) for several values of $Ra \geqslant Ra_c^{(o)}$ for the oscillatory case. The nonlinear interaction between θ_0 and the oscillatory motion is responsible for the $O(1)$ adjustments in θ_0 which result in the development of a broad isothermal interior and thin thermal boundary layers near the top and bottom with increasing Ra. Solutions of this type resemble those obtained elsewhere for a vertical magnetic field (Julien *et al.* 1999*a*).

As the tilt angle is increased the oscillatory solution becomes less efficient at transporting heat, and the Nusselt number has a weaker dependence on Ra as shown in figure 5, although the general form of this dependence continues to resemble the vertical case. The increase in tilt angle leads to a larger Lorentz force, which in

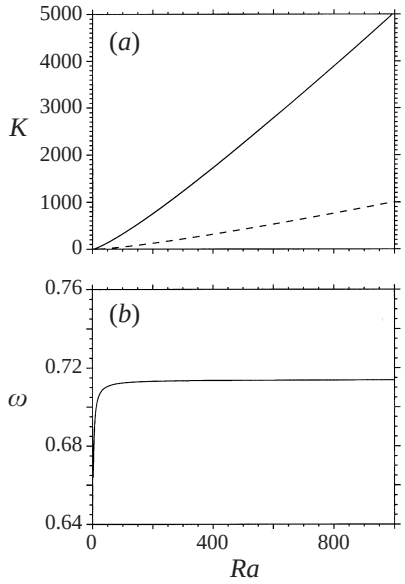

FIGURE 3. (*a*) The (time-averaged) Nusselt number K for steady (dashed line) and oscillatory (solid line) perpendicular rolls as a function of the scaled Rayleigh number Ra when $\zeta = 0.1$, $\sigma = 1.1$ and $\vartheta = \pi/18$. (*b*) The corresponding (scaled) oscillation frequency ω. Note that ω appears to saturate with increasing Ra.

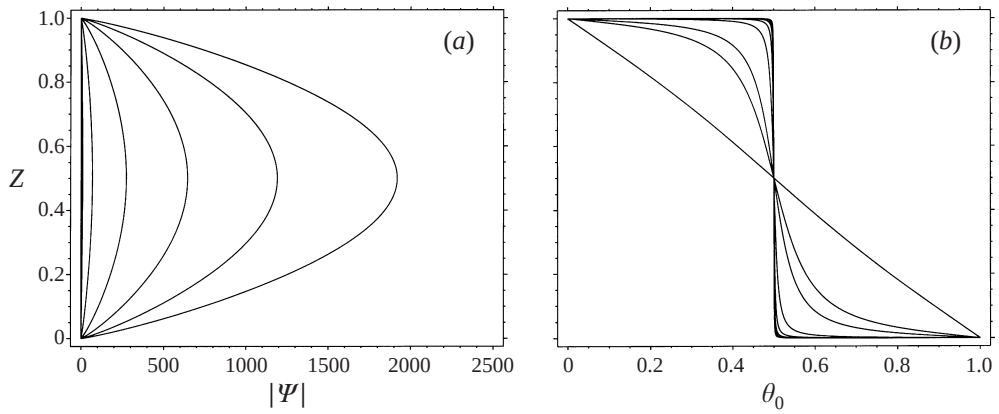

FIGURE 4. (*a*) Convection amplitude for perpendicular rolls as measured by $|\Psi(Z)|$ and (*b*) mean temperature profile $\theta_0(Z)$ for oscillatory convection at (scaled) $Ra = Ra_c$, 2, 6, 10, 50, 170, 370, 650, 1010 showing the development of thin thermal boundary layers and a broad isothermal core with increasing Ra when $\zeta = 0.1$, $\sigma = 1.1$ and $\vartheta = \pi/18$. These properties characterize the 'vertical' convection mode.

turn leads to a suppression of the heat transport. In the steady case the dependence on tilt angle is much weaker. This is to be expected since in the oscillatory regime ohmic diffusion has only a finite time to reduce the Lorentz force due to field distortion before the flow reverses. In contrast, in the steady case the magnetic field perturbation is expelled into narrow boundary layers and the Lorentz force exerts a much weaker effect. In this case the reduction of the Nusselt number is largely due to a geometrical effect: the strong oblique magnetic field inclines the convection cells

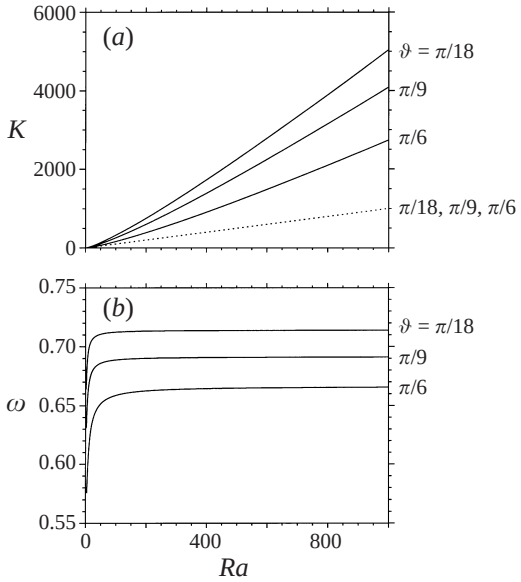

FIGURE 5. (*a*) The (time-averaged) Nusselt number K for steady (dashed lines) and oscillatory (solid lines) perpendicular rolls as a function of the scaled Rayleigh number Ra for several values of the tilt angle ϑ when $\zeta = 0.1$, $\sigma = 1.1$. (*b*) The corresponding (scaled) oscillation frequencies ω. Both K and ω decrease monotonically with increasing ϑ.

relative to the vertical allowing them more time to lose their upward buoyancy to adjacent descending fluid.

Figure 6 shows the corresponding results for the oscillatory mode when $\vartheta = \pi/4$. The figure reveals a remarkable behaviour: the Nusselt number K initially increases rapidly with Ra as in the vertical magnetic field case, but then undergoes a hysteretic transition to a new state characterized by a small Nusselt number, and one that decreases slowly with increasing Ra. As this state is followed to larger Rayleigh numbers we see that the mean temperature becomes almost piecewise linear (figure 7*b*), with a limited isothermal core. The vertical extent of this core quickly saturates, in contrast to the case of a vertical field for which the isothermal core grows continuously with Ra as the temperature gradients are compressed into ever thinner thermal boundary layers (as in figure 4*b*). Evidently, in this state increasing the heat input does not result in increased heat transport across the layer. Instead, as discussed further below, the added energy is all stored in the magnetic field perturbations (since the imposed field strength is large this is achieved with small deformation of the field); moreover, the perturbation magnetic field suppresses the convective motion in the boundary layers near the top and bottom (see figure 7*a*) thereby reducing the transport of heat across the layer. In this regime (i.e. on the branch where the Nusselt number remains low as Ra is increased) the system of perpendicular rolls therefore behaves much more like one with an imposed horizontal field.

Figure 7*b* indicates that the new regime (hereafter the 'horizontal' regime) is characterized by broad thermal boundary layers. This is a simple consequence of the suppression of all flow in these layers (see figure 7*a*) by the perturbation magnetic field. As a result the temperature profile in these boundary layers is linear. For example, equation (5.5) shows that in the top boundary layer $\theta_0 = K(1 - z)$. Since the temperature at the outer edge of the boundary layers is $\theta_0 = 1/2$ their width

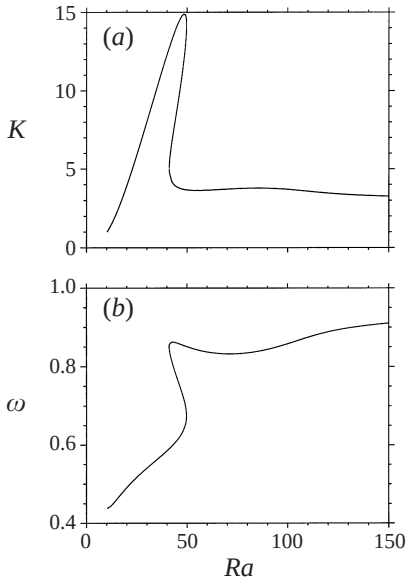

FIGURE 6. (*a*) The (time-averaged) Nusselt number K for oscillatory perpendicular rolls as a function of the scaled Rayleigh number Ra for $\vartheta = \pi/4$ and $\zeta = 0.1$, $\sigma = 1.1$. (*b*) The corresponding frequency ω. Note the hysteretic transition from the 'vertical' convection mode to the 'horizontal' convection mode with increasing Ra.

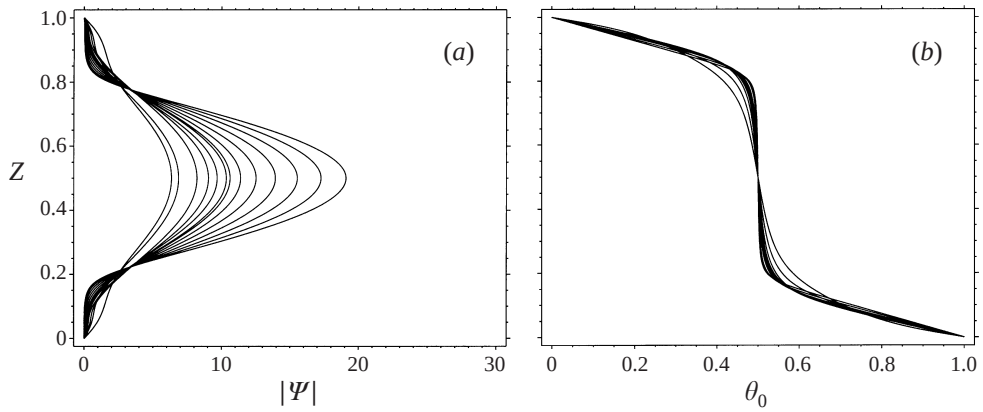

FIGURE 7. (*a*) Convection amplitude as measured by $|\Psi(Z)|$ and (*b*) mean temperature profiles $\theta_0(Z)$ for oscillatory perpendicular rolls at $\vartheta = \pi/4$ (scaled) $Ra = 41.17$, 65.17, 89.17, 113.17, 137.17, 161.17, 171.17, 201.17, 251.17, 321.17, 411.17, 521.17, 651.17, showing the development of broad boundary layers and small isothermal core with increasing Ra when $\zeta = 0.1$, $\sigma = 1.1$. These properties are characteristic of the 'horizontal' convection mode.

is approximately $1/2K$. Moreover, since K is almost independent of the Rayleigh number so is their structure once the Rayleigh number is high enough. This is so despite the fact that the convective amplitude in the isothermal interior continues to increase monotonically with Ra in this regime. As a result the high Rayleigh number asymptotics described by Julien *et al.* (1999*a*) do not break down owing to the formation of $O(Q^{-1/4})$ boundary layers at the top and bottom; such boundary layers only form in steady convection. Note that the Rayleigh number must exceed a

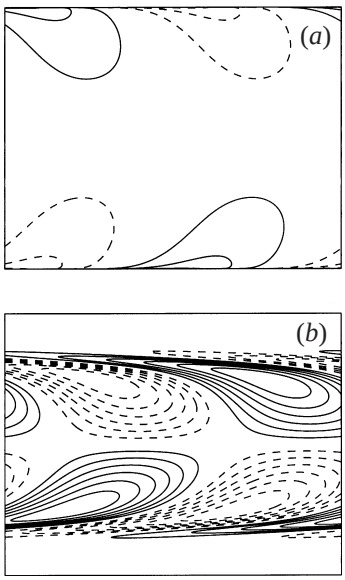

FIGURE 8. Contours of constant $B_1(x,z,Z,t)$ at a particular instant in time on (a) the vertical mode branch when $\vartheta = 10^\circ$ and $Ra = 1010$, and (b) the horizontal mode branch when $\vartheta = 45^\circ$ and $Ra = 738.77$. The parameters are $Q^{1/4}k_{0\perp} = 1.0$, $\zeta = 0.1$ and $\sigma = 1.1$. The magnetic field perturbation peaks close to the boundaries in (a) but defines the outer boundary of the stagnant boundary layers in (b). Solid (dashed) lines indicate positive (negative) values.

critical value before the horizontal convection mode sets in. This is because the flow in the interior must be strong enough to expel the magnetic field perturbation into the boundary layers at the top and bottom; this expulsion occurs primarily in the direction parallel to the field since the velocity in this direction is much larger than the horizontal velocity. In steady convection the resulting boundary layer thickness is determined by the magnetic Reynolds number and is small if this is large. In contrast, in an oscillatory flow the flow reversals prevent the formation of such narrow boundary layers and the boundary layer thickness is determined by the perturbation Lorentz force and not the magnetic Reynolds number. The resulting boundary layers are therefore wider than in the case of steady convection. Support for this interpretation is provided by figure 8 which shows contours of the magnetic flux function $B_1(x,z,Z,t)$ at a particular instant in time for solutions on the vertical and horizontal branches. In the former case the magnetic field perturbation is confined to the vicinity of the top and bottom boundaries; in the latter it peaks at the boundary between the isothermal core and the stagnant boundary layers, and vanishes in the boundary layers themselves, i.e. the field in these boundary layers is the imposed tilted field.

A number of conclusions follow immediately from the above considerations. First, the transition between the two regimes occurs at lower Rayleigh numbers when ϑ is larger. Indeed, for small values of the tilt angle ϑ we have shown that the transition to the lower horizontal branch does not occur (for this value of ζ) but that solutions stay on the efficient vertical branch. Moreover, since the ability of the magnetic field to suppress oscillatory convection increases with decreasing ζ, we expect the value of the Rayleigh number at which the transition from the vertical field regime to the horizontal field regime takes place to be an increasing function of ζ. Figure 9 shows the Rayleigh number at which the vertical branch turns around (i.e. the Rayleigh number $Ra_{\rm SN}$) as a function of ζ for $\vartheta = \pi/4$ confirming this expectation. This

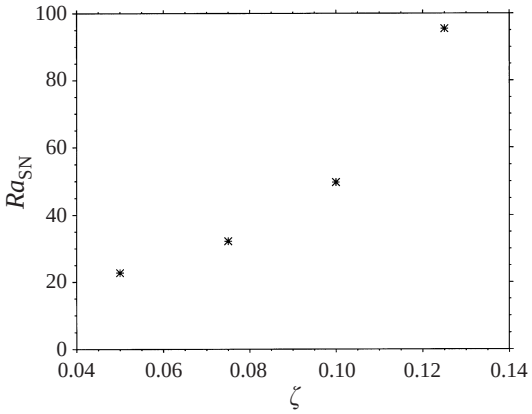

FIGURE 9. The Rayleigh number for the upper saddle-node bifurcation in figure 6 ($\vartheta = \pi/4$) diverges with increasing ζ.

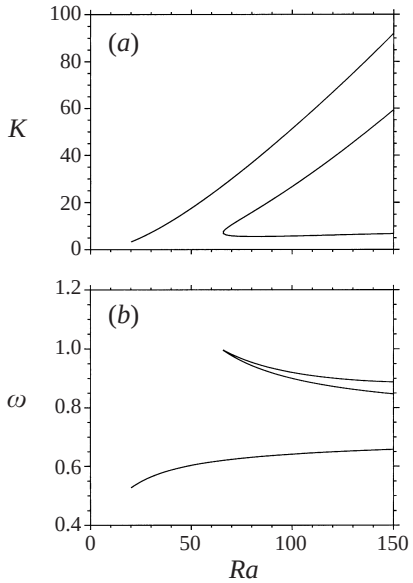

FIGURE 10. (*a*) The (time-averaged) Nusselt number K for oscillatory perpendicular rolls as a function of the scaled Rayleigh number Ra for $\vartheta = \pi/4$ and $\zeta = 0.15$, $\sigma = 1.1$, showing multiple branches. (*b*) The corresponding frequencies ω.

argument also explains why the two convection regimes are only found in oscillatory convection.

In figure 10 we show that if ζ is increased further (to $\zeta = 0.15$) the situation becomes radically different. The vertical field branch now extends to arbitrarily large Rayleigh numbers while the horizontal field branch has become disconnected. The upper saddle-node bifurcation has therefore disappeared. Solutions on the disconnected branch can only be found by continuation in ζ at sufficiently large Ra from the horizontal field solutions obtained with $\zeta = 0.1$ (figure 6). If Ra is then decreased at $\zeta = 0.15$ one follows the horizontal field branch to a saddle-node bifurcation (at $Ra \approx 65.8$), where it turns around. Near this point the character of the solution changes abruptly, and

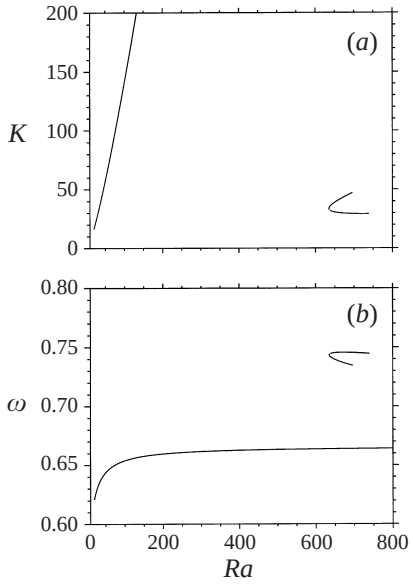

FIGURE 11. As figure 10 but for $\vartheta = 0.5632$ and $\zeta = 0.1$ showing a completely disconnected horizontal branch.

the solutions begin to look like those on the vertical field branch that connects to $K = 1$. Figure 11 shows that the disconnected branch moves away from the vertical branch as the tilt angle is decreased. For these parameter values ($\vartheta = 0.5632 < \pi/4$, $\zeta = 0.1$, $\sigma = 1.1$) the saddle-node bifurcation on the horizontal branch has moved out to $Ra \approx 635$. This result suggests that the critical value of ζ at which the vertical and horizontal field branches disconnect is an increasing function of ϑ; the qualitative theory described in § 6.5 lends support to this suggestion.

In summary, in the perpendicular case ($\chi = 0$) the behaviour of the system falls into two possible regimes. For small tilt angles the magnetic field plays a minor role in inhibiting convection and the Nusselt number is an increasing function of the Rayleigh number. If the tilt angle is increased past a threshold value (which depends on the value of ζ) a hysteretic transition may take place with increasing Rayleigh number from this vertical field regime to a horizontal field regime in which the field plays a major role in inhibiting the heat transport.

Although we do not calculate the stability of these solutions, continuity arguments suggest that in the absence of secondary Hopf and parity-breaking bifurcations (and of sideband instabilities) the upper vertical field branch is stable up to the first saddle-node bifurcation (if present), as is the lower of the two horizontal field branches.

6.2. *Parallel rolls:* $\chi = \pi/2$

As noted earlier, when the imposed field is horizontal and the roll axes parallel to the plane containing the tilted magnetic field it is possible for the fluid to move without distorting the field. This is no longer so when the field is inclined and one expects that in this case the behaviour will resemble that described above for the perpendicular case. This is indeed so, although the transition from the vertical convection mode to the horizontal mode now takes place at larger inclinations ϑ. Figure 12 shows the Rayleigh number dependence of the Nusselt number and oscillation frequency for steady and oscillatory parallel rolls when $\vartheta = \pi/4$, $\zeta = 0.1$ and $\sigma = 1.1$, while figure 13

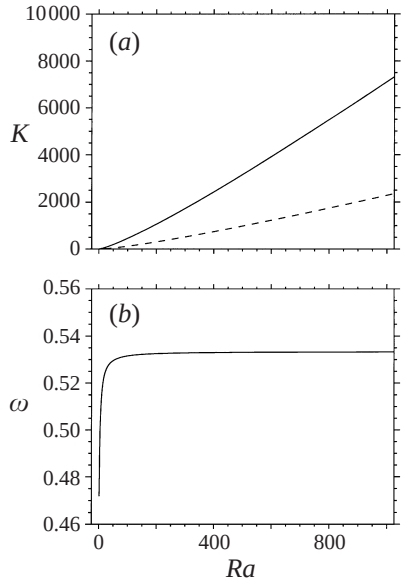

FIGURE 12. (*a*) The (time-averaged) Nusselt number K for steady (dashed line) and oscillatory (solid line) parallel rolls as a function of the scaled Rayleigh number Ra for $\vartheta = \pi/4$ when $\zeta = 0.1$, $\sigma = 1.1$. (*b*) The corresponding (scaled) oscillation frequency ω.

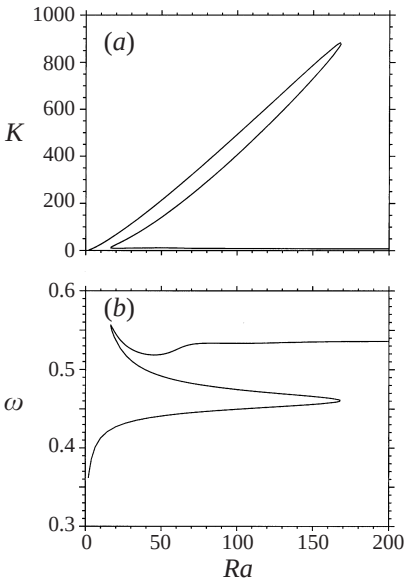

FIGURE 13. As figure 12 but when $\vartheta = 1$ ($\vartheta = 57°$), showing a transition to the horizontal convection mode.

shows the corresponding results for $\vartheta = 1$. In the former case the oscillatory solutions remain on the vertical branch for all values of Ra, while the frequency saturates as Ra increases, in contrast to the behaviour shown in figure 6 for the perpendicular case. However, as shown in figure 13, a transition to the horizontal branch does occur for larger tilt angles, as anticipated in section 1.

The results for rolls inclined at intermediate angles χ are qualitatively similar. For example, for the parameter values of figure 12 and $\chi = \pi/4$ the saddle-node bifurcation on the vertical branch occurs at $Ra_{SN} \approx 66.5$ instead of at $Ra_{SN} \approx 49.73$, the value for $\chi = 0$; when $\chi = \pi/2$ there is no saddle-node bifurcation for $\vartheta = \pi/4$ but for $\vartheta = 1$ $Ra_{SN} \approx 168$.

6.3. *Rectangular patterns*

From symmetry considerations it is clear that a solution with orientation χ is accompanied by another solution with orientation $-\chi$. Consequently it should be possible to find three-dimensional solutions with a rectangular planform. Such solutions can certainly be found at small amplitude. There are two types of steady convection patterns, oblique rolls and rectangles; in the case of overstable patterns there are six solutions that appear generically in the primary Hopf bifurcation (Silber, Riecke & Kramer 1992). These are travelling and standing oblique rolls, two types of travelling rectangles, one type of standing rectangles and a rectangular pattern called alternating rolls. The steady solutions take the form

$$\Psi(\boldsymbol{x}, Z) = \tfrac{1}{2}\Psi(Z)\{a_+ \mathrm{e}^{\mathrm{i}\boldsymbol{k}_1\cdot\boldsymbol{x}} + a_- \mathrm{e}^{\mathrm{i}\boldsymbol{k}_2\cdot\boldsymbol{x}} + \text{c.c.}\}, \tag{6.2}$$

where $\boldsymbol{k}_{1,2} = k_{0\perp}(\cos\chi, \pm\sin\chi, -\cos\chi\tan\vartheta)$. It is easy to check that the projection P still eliminates all nonlinear terms from equations (4.19)–(4.22). However, the fully nonlinear theory carries through only if the two nonlinear terms in (4.24) also vanish. We find that this is so only for oblique rolls ($a_+ = 0$, or $a_- = 0$) or for travelling or standing oblique rolls. Such patterns are two-dimensional and hence described by the nonlinear eigenvalue problems (5.7), (5.8). Thus no fully nonlinear three-dimensional solutions are accessible by the asymptotic method used here.

6.4. *Depth-dependent magnetic diffusivity*

In this section we discuss the effect of prescribing a diffusivity that is a function of depth, i.e. $\zeta \equiv \zeta(Z)$. We follow Weiss *et al.* (1990, 1996) and Julien *et al.* (1999*a*) and choose a linear dependence on depth, $\zeta(Z) = \zeta_0 + \epsilon(1-Z)$. We can think of this depth dependence as a consequence of a depth-dependent ohmic diffusivity, provided we reinterpret the quantity η entering into the definition of the Chandrasekhar number Q as a reference value, for example, measured at mid-depth. The most interesting case arises when ζ changes from favouring oscillatory convection at the top of the layer ($\zeta < 1$) to favouring steady convection at the bottom of the layer ($\zeta > 1$). In the following we therefore choose $\zeta_0 = 0.1$, $\epsilon = 2.0$ and investigate in the perpendicular case $\chi = 0$ changes in the solution as Ra increases for two different values of the tilt angle ϑ.

The vertical field case ($\vartheta = 0$) has been investigated in detail by Julien *et al.* (1999*a*) as a function of the parameter ϵ. The corresponding results for $\vartheta = \pi/4$ are shown in figure 14. The behaviour of both the Nusselt number and frequency with increasing Ra is very similar to that in the vertical case. For the present parameter values the primary bifurcation is a steady-state one but the resulting steady convection loses stability almost immediately to an oscillatory mode. This transition involves a degenerate Takens–Bogdanov bifurcation of the type discussed by Julien *et al.* (1999*a*). As Ra is increased further the oscillatory mode behaves in the usual manner for the vertical branch with K increasing monotonically with Ra and the frequency ω saturating. Because of the up–down asymmetry introduced by the depth dependence of ζ, the solution is no longer symmetric with respect to $Z = 1/2$. Julien *et al.* (1999*a*) show examples of similar solutions for an imposed vertical magnetic field.

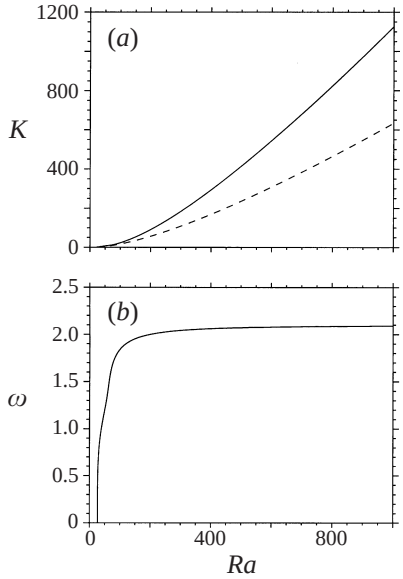

FIGURE 14. (*a*) The (time-averaged) Nusselt number $K(Ra)$ for oscillatory perpendicular rolls when $\vartheta = \pi/4$ and $\zeta(Z) = \zeta_0 + \epsilon(1 - Z)$ with $\zeta_0 = 0.1$ and $\epsilon = 2.0$. (*b*) The corresponding frequency $\omega(Ra)$. The primary instability is a steady-state one but the resulting steady convection (dashed line) loses stability almost immediately to oscillatory convection (solid line).

When the tilt angle is increased further the solution changes drastically in character, as might be expected from the constant-ζ calculations. Figure 15 shows the branches computed for $\vartheta = 5\pi/18 = 50^\circ$ at low Ra. The primary instability is again a steady-state one and gives rise to a monotonically increasing branch of steady solutions, which quickly lose stability to oscillatory convection, exactly as in figure 14. However, at larger Ra (see figure 16) the behaviour is now quite different. Although the Nusselt number for the (unstable) steady branch increases monotonically with Ra, the behaviour of the oscillatory branch is quite complex. After an initial increase in both frequency and K with Ra, the solution behaves for larger values of Ra like a horizontal branch solution of the type described in the previous subsections. The Nusselt number is a weak function of Ra and is non-monotonic. Investigation of the behaviour of the streamfunction $|\Psi(Z)|$ (figure 17*a*) and the corresponding mean temperature $\theta_0(Z)$ (figure 17*b*) shows that after a complicated series of transitions the solution settles down to one in which a largely isothermal core is squeezed between two broad boundary layers characteristic of the horizontal branch. The solution is strongly asymmetric with respect to the midplane $Z = 1/2$ due to the linear dependence of ζ on Z.

Some care must be taken when interpreting these solutions. This is because the depth-dependence of ζ fundamentally changes the symmetry properties of the primitive equations when the imposed field is inclined. Because of the tilt of the field these equations are not equivariant under left–right reflections but when ζ is constant they are equivariant under the combined operation π consisting of a reflection in a vertical plane followed by a reflection in the midplane of the layer. As a result if a left-travelling wave is a solution so is a right-travelling wave, and consequently so are standing waves. Moreover, steady solutions in the form of tilted convection cells are

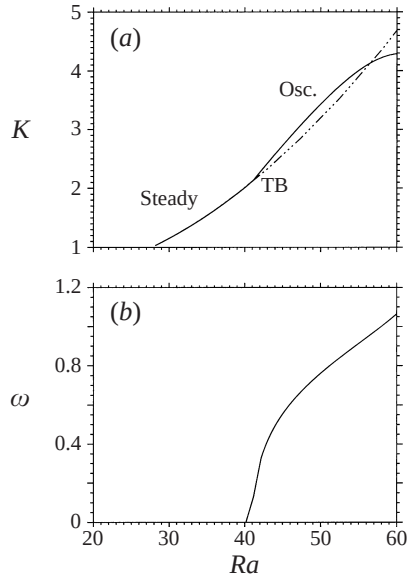

FIGURE 15. (*a*) The (time-averaged) Nusselt number $K(Ra)$ for steady (dot-dashed line) and oscillatory (solid line) perpendicular rolls for $\vartheta = 5\pi/18$ and $\zeta(Z) = \zeta_0 + \epsilon(1 - Z)$ with $\zeta_0 = 0.1$ and $\epsilon = 2.0$. (*b*) The corresponding (scaled) oscillation frequency $\omega(Ra)$. Initially steady convection loses stability to overstable convection at the point labelled TB.

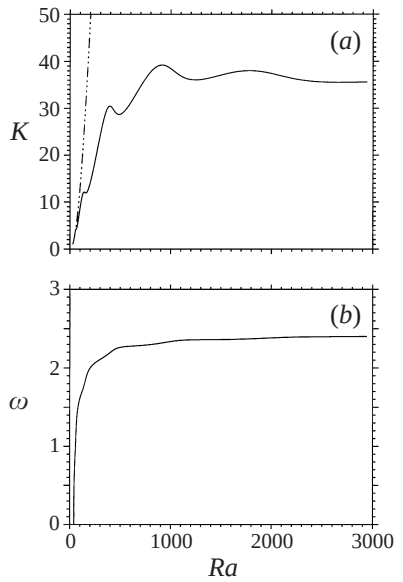

FIGURE 16. As for figure 15 but for a much larger range of Rayleigh numbers, showing the development of the horizontal convection mode.

also possible. We have described solutions of this form in §§ 6.1 and 6.2. However, as noted by Matthews *et al.* (1992) and discussed in more detail by Knobloch (1994), when the properties of the layer depend on depth the midplane symmetry is usually lost and so is the symmetry π. In this case there are generically no steady-state

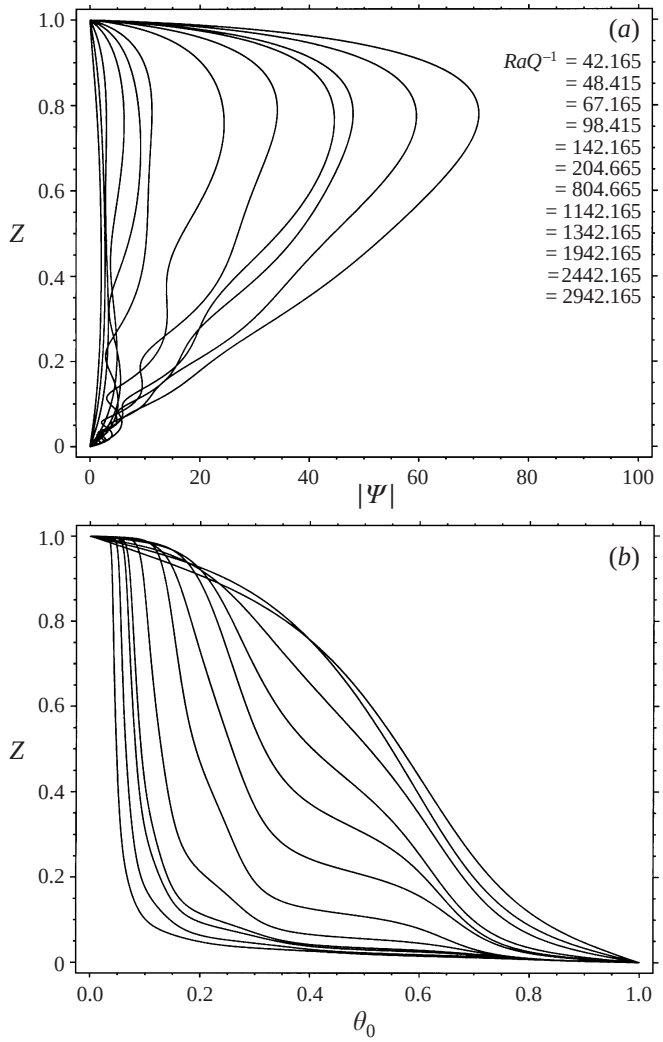

FIGURE 17. The development of (*a*) the convection amplitude $|\Psi(Z)|$ and (*b*) mean temperature profile $\theta_0(Z)$ with scaled Rayleigh number corresponding to figure 15. Note the asymmetry of the profiles.

bifurcations from the conduction state and the primary instability is a Hopf bifurcation to travelling waves with a preferred direction of propagation selected by the tilt together with the depth-dependence. There are also no bifurcations to standing waves, the counterparts of which are quasi-periodic waves that appear in a secondary bifurcation from the primary travelling wave branch. These effects are absent in the large-Q limit because they rely on frequency splitting due to the depth-dependence and this remains of order one, i.e. on the $O(Q^{1/2})$ timescale the drift of our steady solutions is negligible and so is the second frequency accompanying our standing waves, or the frequency difference between left- and right-travelling waves. Likewise, the splitting in the critical Rayleigh numbers for the onset of left- and right-travelling waves remains $O(1)$ and hence small compared to the $O(Q)$ Rayleigh numbers con-

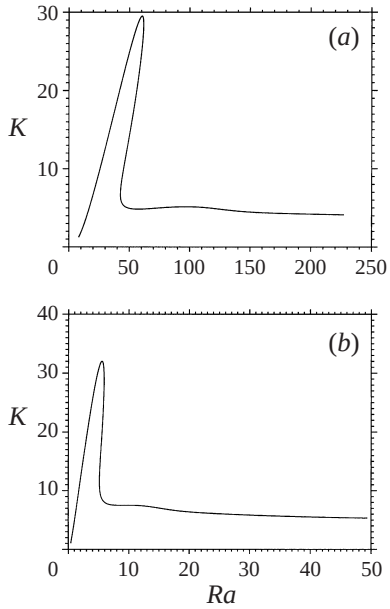

FIGURE 18. The time-averaged Nusselt number K as a function of the scaled Rayleigh number for oscillatory perpendicular rolls with (*a*) $k_0 = 1.0$, $\vartheta = 65°$, $\zeta = 0.1$ and (*b*) $k_{0\perp} = 0.1$, $\vartheta = 75°$ and $\zeta = 0.01$, for comparison with figure 6. In both cases $\sigma = 1.1$.

sidered. It is important to bear these facts in mind when interpreting the solutions just described.

6.5. *Dependence on wavenumber*

Thus far all the results described have been for $k_{0\perp} = 1.0$. Since one may argue, on physical grounds, that the dynamics in an oblique field is determined by the total wavenumber k_0, we have also performed calculations with $k_0 = 1.0$. For $\vartheta = 45°$ we were unable to locate a horizontal branch for values of Ra comparable to those used in figure 6. For larger values of ϑ, however, we found a bifurcation diagram that is qualitatively similar to that shown in figure 6 (see figure 18*a*). In particular both the vertical and the horizontal branches are still present, as is the hysteresis loop separating them.

In weakly nonlinear theories of pattern selection the wavenumber of the pattern is usually taken to be the one that minimizes the critical Rayleigh number for onset. Although there is no reason for making this choice in a fully nonlinear theory such as that described in this paper it is nonetheless of interest to examine the results for this special choice of $k_{0\perp}$. As indicated in § 3 the neutral stability curve is very flat in the scaled variables but its minimum occurs at $O(Q^{1/6})$ in unscaled variables, corresponding to the limit $k_{0\perp} \to 0$ in the scaled variables used here. In this limit the problem (5.8) reduces to

$$\mathrm{D}^2\Psi_0 + \frac{\omega_0^2}{r_z^2\sigma\zeta}\Psi_0 + \frac{Ra\,K_0}{r_z^2\zeta\gamma}\frac{1}{1+2\gamma|\Psi_0|^2}\Psi_0 = 0, \tag{6.3}$$

where $\gamma \equiv k_0^2/k_{0\perp}^2$, and the frequency ω and the time-averaged Nusselt number K_0

are given by

$$\omega_0^2 = \frac{r_z^2 \sigma \zeta (1-\zeta)}{1+\sigma} \frac{\int_0^1 |\mathrm{D}\Psi_0|^2 \,\mathrm{d}z}{\int_0^1 |\Psi_0|^2 \,\mathrm{d}z} \tag{6.4}$$

and

$$K_0^{-1} = \int_0^1 \frac{1}{1+2\gamma|\Psi_0|^2} \,\mathrm{d}z. \tag{6.5}$$

The result (6.4) follows from the solvability condition for the imaginary part of Ψ_2, where $\Psi = \Psi_0 + k_{0\perp}^2 \Psi_2 + \cdots$; inessential factors have been absorbed into a rescaling of Ψ_0 which can be taken to be real. Equation (6.4) agrees with that obtained by Matthews (1999) for vertical magnetic field ($r_z = 1$) and $O(Q^{1/6})$ wavenumbers. Defining $\Omega_0 \equiv \omega_0 / r_z$ we obtain an eigenvalue problem for $Ra/\gamma r_z^2$. As a consequence for perpendicular rolls K_0 is independent of ϑ, while the frequency scales with $\cos\vartheta$. The solutions of the eigenvalue problem that arises if the limit $k_0 \to 0$ is taken instead can be obtained from the above one on replacing γ by γ^{-2} and $Ra\gamma^3$ by Ra, namely

$$\mathrm{D}^2\Psi_0 + \frac{\omega_0^2}{r_z^2 \sigma \zeta}\Psi_0 + \frac{Ra\, K_0}{r_z^2 \zeta} \frac{\gamma}{\gamma^2 + 2|\Psi_0|^2}\Psi_0 = 0, \tag{6.6}$$

with ω given by (6.4) and

$$K_0^{-1} = \int_0^1 \frac{\gamma^2}{\gamma^2 + 2|\Psi_0|^2} \,\mathrm{d}z. \tag{6.7}$$

The solution of the problem (6.6) with (6.4), (6.7) behaves in a qualitatively similar way to the finite-k_0 problem: the frequency ω_0 saturates with increasing Ra and the numerical value agrees with that obtained by Matthews (1999) for $\vartheta = 0$,† while the Nusselt number still increases as $Ra \ln Ra$.

Figure 18(*b*) shows the effect of decreasing $k_{0\perp}$ on the transition to the horizontal regime for perpendicular rolls. In order to locate this regime for $k_{0\perp} = 0.1$ we found it necessary to both decrease ζ and increase the tilt angle ϑ. On the basis of a number of calculations with different values of $k_{0\perp}$ and k_0 we conjecture that, for sufficiently small ζ, there is always a value of ϑ for which the bifurcation diagram develops a horizontal branch with increasing Ra. However, for fixed ζ and σ, the tilt angle which minimizes the Rayleigh number at which this branch first develops depends on the wavenumber chosen. These conclusions are in agreement with a qualitative argument for the presence of the horizontal regime. This argument is based on the requirement that the flow in each tilted cell is sufficiently strong to transport magnetic field perturbations into horizontal boundary layers along the top and bottom boundaries. In a time-dependent flow this requirement takes the form $c_p \lesssim U^*$, where $c_p \equiv \omega/(k_{0z}\cos\vartheta)$ is the phase velocity parallel to the magnetic field and U^* is the corresponding parallel flow velocity (cf. Knobloch & Merryfield 1992). Note that in unscaled variables $\omega = O(Q^{1/2})$, and $k_{0z} = O(Q^{1/4})$, while $U^* = O(Q^{1/4})$, indicating that this requirement is independent of the magnetic field strength. Since $U^* = O(k_{0\perp}^2 \Psi / \cos\vartheta)$ while for large Ra (and small k_0) $Ra \sim \pi(\zeta\lambda)^{1/2}\Psi(2\ln\Psi)^{-1/2}$ where $\lambda \equiv \lambda(\zeta, \vartheta)$ is independent of Ra (Julien *et al.* 1999*a*), we conclude that for

† Figure 5 of Matthews (1999) shows ω^2 as a function of Ra/Q, not ω.

perpendicular rolls

$$k_{0\perp} \gtrsim \omega_\infty^{1/3} \left(\frac{\cos^2 \vartheta}{\sin \vartheta} \right)^{1/3} (\zeta \lambda)^{1/6} Ra^{-1/3}. \tag{6.8}$$

To obtain this result we omitted logarithmic corrections and constants of order one, and approximated the oscillation frequency at large Ra by $\omega_\infty \cos \vartheta$, where ω_∞ is a constant independent of both Ra and ϑ; in magnitude this constant is of the order of $\pi[\sigma\zeta(1-\zeta)/(1+\sigma)]^{1/2}$. To examine the ϑ dependence of the requirement (6.8) we need to determine the ϑ dependence of λ. This follows from (6.3) which shows that, for large Ra, $\Psi \propto \cos \vartheta$ while K is ϑ-independent. Thus $\lambda \sim \lambda_\infty(\zeta)/\cos^2 \vartheta$. Moreover, Julien *et al.* (1999*a*) show that λ_∞ decreases with decreasing ζ. The condition (6.8) thus becomes

$$k_{0\perp} \gtrsim \omega_\infty^{1/3} (\cot \vartheta)^{1/3} (\zeta \lambda_\infty)^{1/6} Ra^{-1/3}. \tag{6.9}$$

It follows that if we decrease $k_{0\perp}$ we must increase Ra substantially in order to observe the transition to the horizontal regime. Moreover, for a given value of $k_{0\perp}$, increasing ϑ or decreasing ζ should reduce the value of Ra at which this transition takes place. These predictions are also consistent with our numerical results (see figure 18*b*). The condition (6.9) can also be written in the form

$$k_0 \gtrsim \omega_\infty^{1/3} (\sin \vartheta \cos^2 \vartheta)^{-1/3} (\zeta \lambda_\infty)^{1/6} Ra^{-1/3}, \tag{6.10}$$

indicating that for fixed k_0 it is not possible to find the transition to the horizontal regime simply by varying ϑ if the Rayleigh number is insufficiently large. These predictions agree with our numerical calculations: when $k_0 = 0.1$ we were unable to locate a horizontal branch in the Rayleigh number range used in figure 18(*b*) for any value of ϑ even when $\zeta = 0.01$. It is possible that reducing ζ even further as suggested by the above argument could help.

In the parallel case the wave does not propagate in the x-direction and there is no difference between $k_{0\perp}$ and k_0. The transport mechanism is therefore changed from that associated with a propagating wave to one characteristic of a standing wave. In the present case the (unscaled) frequency of the wave is $O(Q^{1/2})$ and the ohmic diffusivity in such a rapidly oscillating (shear) flow is enhanced by the factor $1 + (1/2)(k_0^3 \Psi/\omega)^2$ (cf. Knobloch & Merryfield 1992). In this case the asymptotic eigenvalue problem (6.3) indicates that $\lambda \Psi^2 \propto \cos^2 \vartheta$ while $Ra \sim \pi(\zeta\lambda)^{1/2} \Psi (2 \ln \Psi)^{-1/2} \cos \vartheta$. As a result no reliable conclusion can be drawn from the leading-order asymptotics. Numerically, we were unable to locate the horizontal branch for any ϑ when $k_{0\perp} = 0.1$ or $k_0 = 0.1$ for values of ζ as low as 0.01.

7. Transport properties of tilted rolls

In this section we compute the mean horizontal flow, heat flux and magnetic field associated with magnetoconvection in the presence of oblique fields. In this section we reserve the overbar for horizontal averages and denote time-averages by a superscript t.

The mean equations obtained from the horizontally averaged unscaled governing equations are

$$\frac{1}{\sigma} \partial_t \overline{\boldsymbol{U}}_\perp + \mathrm{D}(\overline{w \boldsymbol{u}_\perp}) = \zeta Q \left(\cos \vartheta \mathrm{D} \overline{\boldsymbol{B}}_\perp + \mathrm{D}(\overline{b_z \boldsymbol{b}_\perp}) \right) + \mathrm{D}^2 \overline{\boldsymbol{U}}_\perp, \tag{7.1}$$

$$\partial_t \overline{\boldsymbol{B}}_\perp + \mathrm{D}(\overline{w \boldsymbol{b}_\perp}) = \cos \vartheta \mathrm{D} \overline{\boldsymbol{U}}_\perp + \mathrm{D}(\overline{b_z \boldsymbol{u}_\perp}) + \mathrm{D}(\zeta \mathrm{D} \overline{\boldsymbol{B}}_\perp), \tag{7.2}$$

with a similar equation from the temperature equation. There is no mean vertical velocity: the vertical components of (7.1) are in equilibrium with a mean vertical pressure gradient. Since $\boldsymbol{u} \sim O(Q^{1/4})$, $\boldsymbol{b} \sim O(Q^{-1/4})$ in all three directions the mean components must scale according to $\overline{\boldsymbol{U}}_\perp \sim O(1)$, $\overline{\boldsymbol{B}}_\perp \sim O(Q^{-1/2})$. As mentioned in § 2 these mean quantities are small and can therefore be determined self-consistently from the fluctuating components. Recalling that $\partial_t \sim O(Q^{\frac{1}{2}})$, the leading-order balance gives

$$\zeta \cos\vartheta \mathrm{D}\overline{\boldsymbol{B}}_\perp = \frac{1}{\sigma}\partial_t \overline{\boldsymbol{U}}_\perp + \mathrm{D}(\overline{w\boldsymbol{u}_\perp} - \zeta\overline{b_z \boldsymbol{b}_\perp}), \tag{7.3}$$

$$\cos\vartheta \mathrm{D}\overline{\boldsymbol{U}}_\perp = \partial_t \overline{\boldsymbol{B}}_\perp + \mathrm{D}(\overline{w\boldsymbol{b}_\perp} - \overline{b_z \boldsymbol{u}_\perp}), \tag{7.4}$$

in scaled variables. The DC components of the mean fields are now obtained by averaging over time and integrating with respect to Z. These expressions can be written in terms of the time-averaged components of the Reynolds stress tensor, $\boldsymbol{R}_{ij} \equiv \overline{u_i u_j} Q^{1/2}$, the magnetic stress tensor, $\boldsymbol{M}_{ij} \equiv \overline{b_i b_j} Q^{-1/2}$, and the mixed stress tensor, $\tau_{ij} \equiv \overline{u_i b_j}$:

$$\overline{\boldsymbol{B}}^t_\perp = \frac{\overline{\boldsymbol{R}}^t_{3\perp} - \zeta \overline{\boldsymbol{M}}^t_{3\perp}}{\zeta \cos\vartheta} Q^{-1/2}, \qquad \overline{\boldsymbol{U}}^t_\perp = \frac{\overline{\tau}^t_{3\perp} - \overline{\tau}^t_{\perp 3}}{\cos\vartheta}. \tag{7.5}$$

Note that the mean magnetic field is determined from the equation of motion, while the mean flow comes from the induction equation. Since $\overline{\boldsymbol{B}}^t_\perp$, $\overline{\boldsymbol{U}}^t_\perp$ are both produced in response to convection no constants of integration appear in these expressions.

Finally, we also introduce the heat flux $\boldsymbol{F}_i \equiv \overline{u_i \theta}$ whose horizontal component is the mean horizontal heat flux.

7.1. *The stress tensors*

Expressions (7.5) require that we evaluate the components of the three tensors just introduced. We find that all components of these quantities can be expressed in terms of

$$R_{33} = 2k_{0\perp}^4 \left[|\Psi|^2 + \frac{c}{1+c^2}\Psi^2 \mathrm{e}^{2\mathrm{i}\omega t} + \frac{c}{1+c^2}\Psi^{*2}\mathrm{e}^{-2\mathrm{i}\omega t} \right] Q^{1/2}, \tag{7.6}$$

$$M_{33} = 2k_{0\perp}^4 \left[|B|^2 + \frac{c}{1+c^2}B^2 \mathrm{e}^{2\mathrm{i}\omega t} + \frac{c}{1+c^2}B^{*2}\mathrm{e}^{-2\mathrm{i}\omega t} \right] Q^{-1/2}, \tag{7.7}$$

$$\tau_{33} = 2k_{0\perp}^4 \left[\tfrac{1}{2}(\Psi B^* + \Psi^* B) + \frac{c}{1+c^2}\Psi B \mathrm{e}^{2\mathrm{i}\omega t} + \frac{c}{1+c^2}\Psi^* B^* \mathrm{e}^{-2\mathrm{i}\omega t} \right], \tag{7.8}$$

$$F_3 = 2k_{0\perp}^2 \left[\tfrac{1}{2}(\Psi \Theta^* + \Psi^* \Theta) + \frac{c}{1+c^2}\Psi \Theta \mathrm{e}^{2\mathrm{i}\omega t} + \frac{c}{1+c^2}\Psi^* \Theta^* \mathrm{e}^{-2\mathrm{i}\omega t} \right], \tag{7.9}$$

with $c = 0$ for travelling waves and steady solutions ($\omega = 0$), and $c = 1$ for standing waves. In particular $\boldsymbol{R} \equiv (R_{11}, R_{12}, R_{13}, R_{22}, R_{23}, R_{33})$ is given by

$$\boldsymbol{R} = \left[\frac{k_{0x}^2 k_{0z}^2}{k_{0\perp}^4}, \frac{k_{0x} k_{0y} k_{0z}^2}{k_{0\perp}^4}, -\frac{k_{0x} k_{0z}}{k_{0\perp}^2}, \frac{k_{0y}^2 k_{0z}^2}{k_{0\perp}^4}, -\frac{k_{0y} k_{0z}}{k_{0\perp}^2}, 1 \right] R_{33}, \tag{7.10}$$

with similar expressions for the magnetic and mixed tensors. The heat flux vector is given by

$$\boldsymbol{F} = \left[-\frac{k_{0x} k_{0z}}{k_{0\perp}^2}, -\frac{k_{0y} k_{0z}}{k_{0\perp}^2}, 1 \right] F_3. \tag{7.11}$$

Note that R_{33} measures the kinetic energy in vertical motions, while M_{33} measures the magnetic energy in the vertical field perturbations and F_3 is the vertical convective heat flux.

For the computation of the horizontal mean flows we need the following higher-order terms as well:

$$\tau_{j3} = k_{0j}k_{0\perp}^2 \frac{1-c^2}{1+c^2}(\mathrm{i}\mathrm{D}\Psi B^* - \mathrm{i}\mathrm{D}\Psi^* B)Q^{-1/4}, \tag{7.12}$$

$$\tau_{3j} = k_{0j}k_{0\perp}^2 \frac{1-c^2}{1+c^2}(\mathrm{i}\mathrm{D}B\Psi^* - \mathrm{i}\mathrm{D}B^*\Psi)Q^{-1/4}, \tag{7.13}$$

$j = 1, 2$. When $\chi = 0$ (perpendicular rolls) these terms are subdominant but are nonetheless necessary for the mean flow computation. When $\chi = \pi/2$ (parallel rolls) both k_{0x} and k_{0z} vanish, and $k_{0y} = k_{0\perp}$. In this case the only non-zero components of the stress tensor and flux at leading order are the 33 and 3 components, respectively, and it is necessary to carry the calculations to next order. In addition to (7.12), (7.13) these lead to the formally subdominant contributions

$$R_{22} = 2k_{0\perp}^2 \left[|\mathrm{D}\Psi|^2 + \frac{c}{1+c^2}(\mathrm{D}\Psi)^2 \mathrm{e}^{2\mathrm{i}\omega t} + \frac{c}{1+c^2}(\mathrm{D}\Psi^*)^2 \mathrm{e}^{-2\mathrm{i}\omega t} \right], \tag{7.14}$$

$$R_{23} = k_{0\perp}^3 \frac{1-c^2}{1+c^2}(\mathrm{i}\mathrm{D}\Psi\Psi^* - \mathrm{i}\mathrm{D}\Psi^*\Psi)Q^{1/4}, \tag{7.15}$$

$$M_{22} = 2k_{0\perp}^2 \left[|\mathrm{D}B|^2 + \frac{c}{1+c^2}(\mathrm{D}B)^2 \mathrm{e}^{2\mathrm{i}\omega t} + \frac{c}{1+c^2}(\mathrm{D}B^*)^2 \mathrm{e}^{-2\mathrm{i}\omega t} \right] Q^{-1}, \tag{7.16}$$

$$M_{23} = k_{0\perp}^3 \frac{1-c^2}{1+c^2}(\mathrm{i}\mathrm{D}BB^* - \mathrm{i}\mathrm{D}B^*B)Q^{-3/4}, \tag{7.17}$$

$$F_2 = k_{0\perp} \frac{1-c^2}{1+c^2}(\mathrm{i}\mathrm{D}\Psi\Theta^* - \mathrm{i}\mathrm{D}\Psi^*\Theta)Q^{-1/4}. \tag{7.18}$$

The remaining quantities all vanish. Moreover, with the exception of R_{22} and M_{22}, the remaining quantities are non-zero only for travelling waves, as expected from symmetry considerations.

7.2. *Results*

In figure 19 we show, for left-travelling waves with (*a*) $\chi = 0$ (perpendicular case) and (*b*) $\chi = \pi/2$ (parallel case), the maximum value of the stress components R_{33}, M_{33}, τ_{33} and F_3 as a function of the Rayleigh number and various tilt angles, all for $k_{0\perp} = 1.0$. These quantities determine all the other leading-order components as indicated in equations (7.10), (7.11). The transition from the vertical field regime to the horizontal one that occurs at large enough tilt angles is clearly visible in both cases. We see that in the horizontal regime the vertical convective heat flux F_3 continues to decrease with Ra while the magnetic perturbation energy M_{33} builds up. These results confirm the physical interpretation of the horizontal field branch given in § 6.1, i.e. in this convection mode the input energy is primarily stored as magnetic energy instead of being transported through the layer by fluid motion. In contrast, for fixed ϑ on the vertical branch all components increase monotonically with Ra. Note that in the perpendicular case all components on the vertical branch decrease monotonically with increasing ϑ at fixed Ra but that this is not so in the parallel case. The corresponding behaviour for steady convection is much simpler

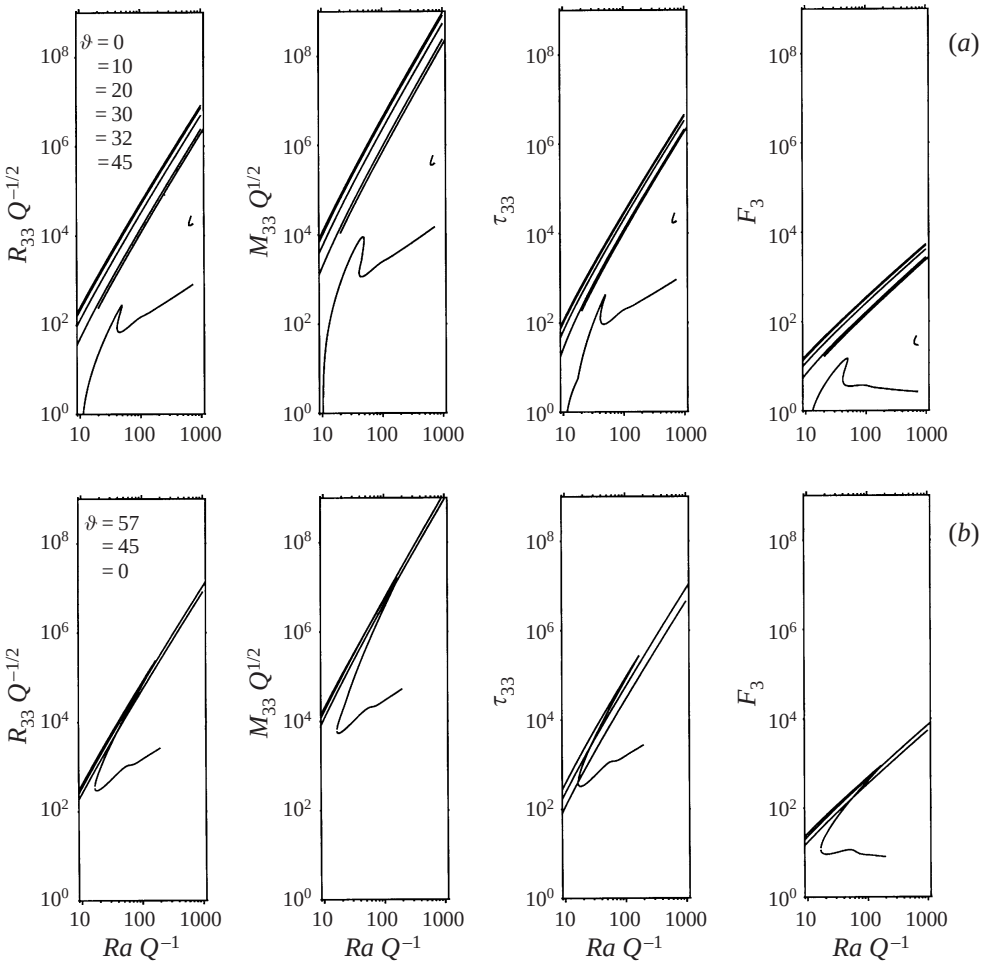

FIGURE 19. The maximum values of the time-averaged Reynolds stress $\overline{R_{33}(Z)}^t$, magnetic stress $\overline{M_{33}(Z)}^t$, mixed stress $\overline{\tau_{33}(Z)}^t$, and the vertical convective heat flux $\overline{F_3(Z)}^t$ for left-travelling waves as functions of Ra for (*a*) $\chi = 0$, (*b*) $\chi = \pi/2$ and various ϑ. The remaining parameters are as for figure 6.

and resembles that found in the oscillatory case for the vertical convection mode. In figure 20(*a*, *b*) we show the vertical profiles of the dominant stress components for both the vertical and horizontal regimes when $\chi = 0$ which further highlight these facts. A comparison of the profiles of M_{33} and of F_3 is particularly useful. On the vertical field branch the perturbation magnetic energy peaks at the top and bottom, indicating that the magnetic field in the bulk is essentially the imposed inclined field. At the same time the convective flux F_3 is almost independent of z. On the horizontal field branch, however, the convective flux is constant only in the small convective core, and falls to zero in the stagnant boundary layers at the top and bottom. At the same time the perturbation magnetic energy is small in the convective core and the stagnant boundary layers, indicating the prevalence of the imposed field in these regions, but peaks in the transition regions outside the core. In these regions a substantial perturbation of the vertical field component is present, due primarily to the recirculation of the field-aligned flow that takes place there. Finally, as shown in

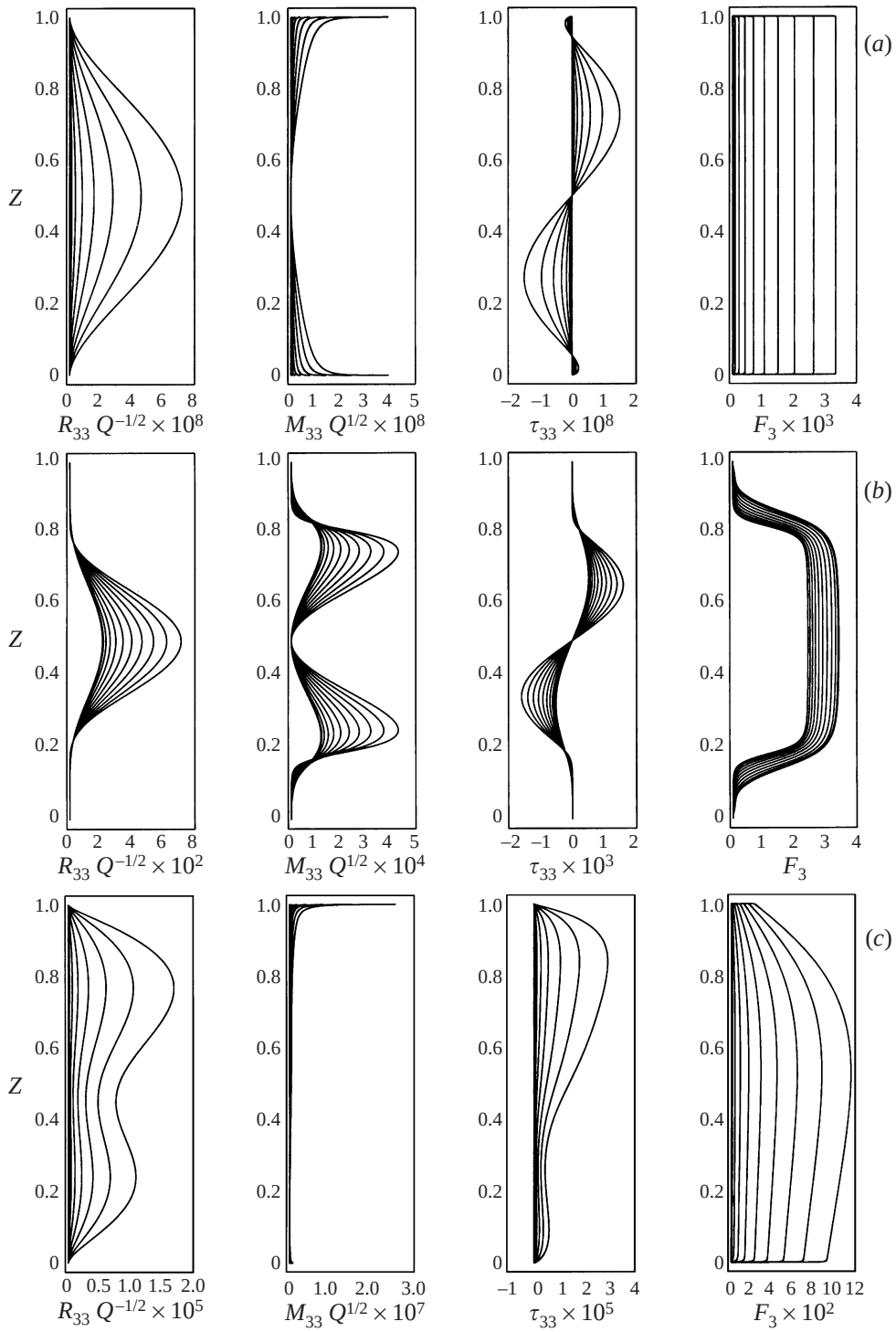

FIGURE 20. Vertical profiles of $\overline{R_{33}(Z)}^t$, $\overline{M_{33}(Z)}^t$, $\overline{\tau_{33}(Z)}^t$ and $\overline{F_3(Z)}^t$ for left-travelling waves when $\chi = 0$ on (*a*) the vertical branch when $\vartheta = 10^\circ$, and (*b*) the horizontal branch when $\vartheta = \pi/4$. (*c*) The corresponding results for variable ζ and the parameters of figure 14 when $\vartheta = \pi/4$.

figure 20(*c*), the transport becomes asymmetric with respect to the midplane when ζ becomes z-dependent. Observe that the convective heat flux is reduced in the upper third of the layer. This is because the vertical velocity is reduced by the build-up of magnetic field in this region. This build-up arises because the smaller value of ζ in this region allows for more concentrated magnetic fields (the magnetic Reynolds number is higher) and hence for a stronger Lorentz force. The pumping of flux into this region is also reflected in the mixed tensor component τ_{33}. Of particular interest is the development of a double peak structure in the vertical kinetic energy R_{33} as Ra increases. This is a consequence of two competing effects. In the low-ζ region near the top the boundary layer structure is dominated by the Lorentz force, while in the lower third of the layer the diffusive timescale is short enough to form essentially diffusive boundary layers. The deformation of the imposed field in the top third increases with Ra and allows for increased vertical (as opposed to oblique) motion; at the same time the lower boundary layer becomes thinner and the resulting field-reduced region favours more vigorous convection in the lower third of the layer. Some tendency towards solutions of this type can be seen in the simulations of compressible magnetoconvection in a horizontal magnetic field by Brownjohn *et al.* (1995). These results remain qualitatively valid for parallel rolls as well.

We are now in a position to evaluate the mean horizontal flow and magnetic field. Calculation of the former requires that we include second-order contributions in the mixed stress tensor. We obtain

$$\overline{\boldsymbol{U}}_j^t = \frac{k_{0j}k_{0\perp}^2}{\cos\vartheta}\left(\frac{1-c^2}{1+c^2}\right)\mathrm{D}(\mathrm{i}B\Psi^* - \mathrm{i}B^*\Psi)Q^{-1/4}. \tag{7.19}$$

This result implies that DC mean flows are only generated by travelling wave convection. However, standing wave solutions drive an AC component of the mean fields of the form $(\overline{\boldsymbol{B}}_\perp, \overline{\boldsymbol{U}}_\perp) = (\hat{\overline{\boldsymbol{B}}}_\perp, \hat{\overline{\boldsymbol{U}}}_\perp)(Z)\mathrm{e}^{2\mathrm{i}\omega t}$. The vertical profiles are determined from

$$\zeta\cos\vartheta\mathrm{D}\hat{\overline{\boldsymbol{B}}}_\perp - \frac{2\mathrm{i}\omega}{\sigma}\hat{\overline{\boldsymbol{U}}}_\perp = \mathrm{D}(\overline{\boldsymbol{R}}_{3\perp} - \zeta\overline{\boldsymbol{M}}_{3\perp})_{2\omega}, \tag{7.20}$$

$$\cos\vartheta\mathrm{D}\hat{\overline{\boldsymbol{U}}}_\perp - 2\mathrm{i}\omega\hat{\overline{\boldsymbol{B}}}_\perp = \mathrm{D}(\overline{\tau}_{3\perp} - \overline{\tau}_{\perp 3})_{2\omega}. \tag{7.21}$$

In figure 21 we show the mean horizontal magnetic field and velocity for oscillatory perpendicular rolls in the form of left-travelling waves (figure 21*a*, *b*) and compare the results with those for perpendicular rolls and variable ζ (figure 21*c*), and parallel rolls (figure 21*d*). On the vertical field branch the largest mean field is found at the top and bottom, and the largest flow at midlevel (figure 21*a*); on the horizontal branch the mean field and velocity are both nearly zero in the stagnant boundary layers at the top and bottom, with current sheets developing with increasing Ra in the transition region between these layers and the convective core (figure 21*b*). In both cases the mean field near the top and bottom is opposite to the horizontal component of the imposed magnetic field, but is parallel to it at midlevel. On the vertical field branch the accompanying mean flow is retrograde (opposite to the net mean flow) at the top and bottom, but prograde at midlevel, while on the horizontal field branch it is prograde everywhere. When ζ depends on z the largest mean fields and velocities develop in regions of smallest ζ as illustrated in figure 21(*c*). In the case of parallel rolls on the vertical branch the mean field that develops is in the y-direction and is antisymmetric with respect to midlevel, in contrast to the perpendicular case. However, the largest mean fields are still produced near the top and bottom boundaries, while the mean

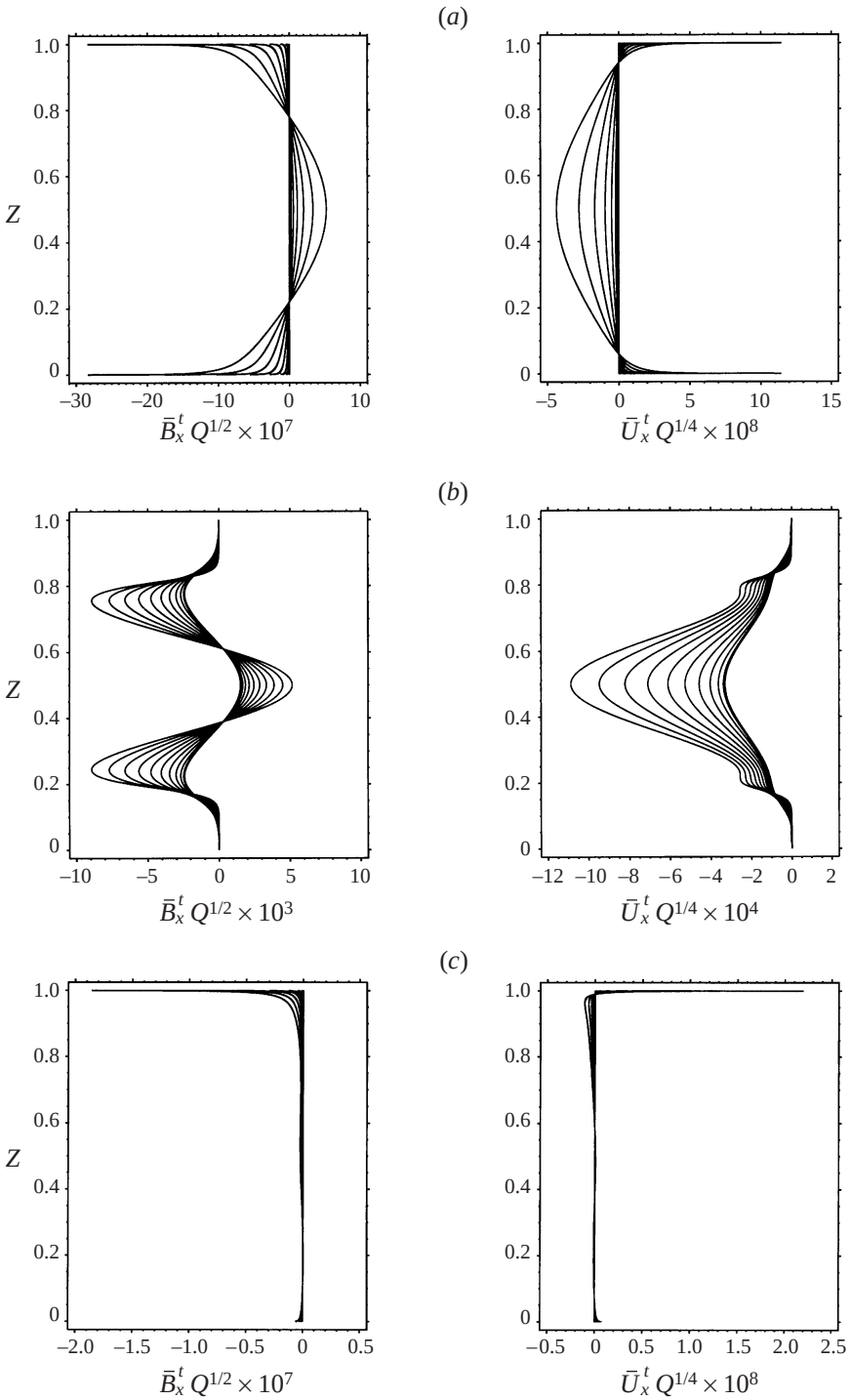

FIGURE 21 (*a–c*). For caption see facing page.

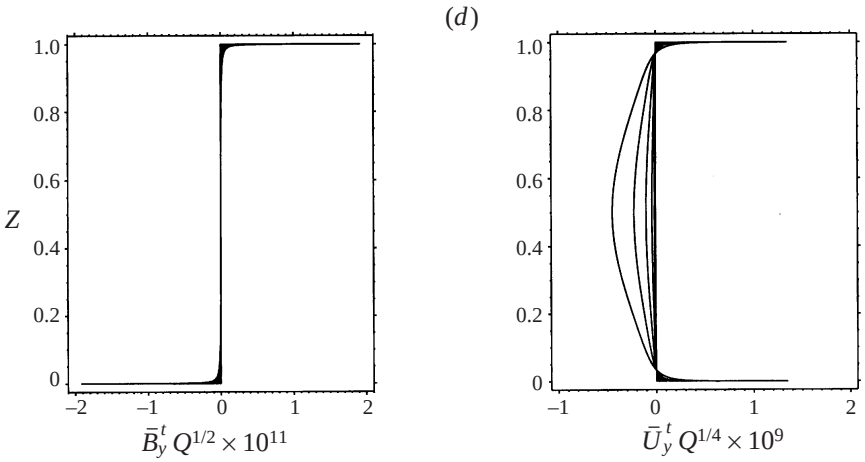

FIGURE 21. Vertical profiles of the mean horizontal magnetic field $\overline{B_\perp(Z)}^t$ and velocity $\overline{U_\perp(Z)}^t$ generated by left-travelling waves in a tilted magnetic field for several values of *Ra*. (*a*) Perpendicular rolls on the vertical branch when $\vartheta = \pi/18$, (*b*) perpendicular rolls on the horizontal branch when $\vartheta = \pi/4$, (*c*) perpendicular rolls with variable ζ when $\vartheta = \pi/4$, and (*d*) parallel rolls when $\vartheta = \pi/4$. The remaining parameters are as in figure 20.

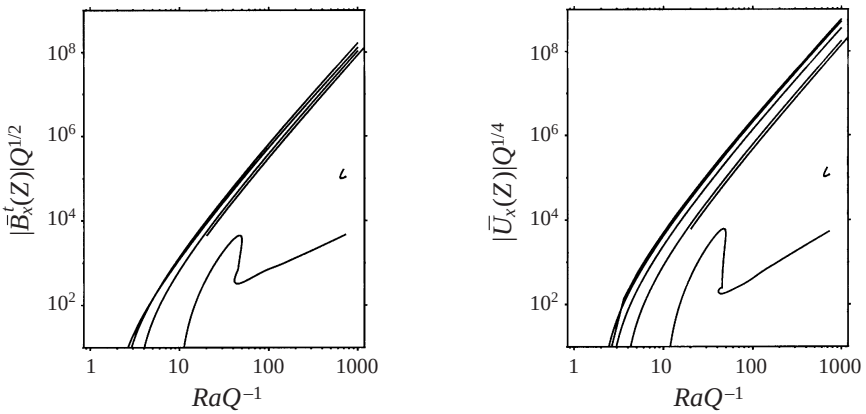

FIGURE 22. The maximum values of the time-averaged (*a*) mean horizontal magnetic field $\overline{B_x(Z)}^t$, and (*b*) mean horizontal flow $\overline{U_x(Z)}^t$ generated by left-travelling waves in the perpendicular case, as a function of *Ra*. From top to bottom $\vartheta = 0$, 10°, 20°, 30°, 32°, 45°.

flow still peaks at midlevel and is predominantly prograde. We do not show the corresponding AC components for standing waves.

Figure 22 shows the maximum value of $|\overline{\boldsymbol{B}}_\perp^t|$ and $|\overline{\boldsymbol{U}}_\perp^t|$ as a function of *Ra* for left-travelling waves in the perpendicular case. In the vertical regime ($\vartheta < 30°$) maximal field generation occurs at $\theta \sim 20°$ but the horizontal flow peaks when $\vartheta = 0$, i.e. for vertical imposed field. This is a manifestation of increasing decorrelation between the velocity and magnetic field with increasing ϑ, as measured by the mixed stress tensor from which the mean flows are determined.

The preceding results suggest that the generation of mean flows by oscillatory convection is a surface phenomenon. Note, however, that no mean flows are generated by steady convection in the present asymptotic limit, although such flows are known to accompany tilted convection cells of the type studied by Matthews *et al.* (1993).

8. Discussion

In this paper we have investigated in detail the transport properties of fully nonlinear convection in an inclined strong magnetic field. For moderate values of the tilt angle of the field the scale of the convection cells transverse to the field is small and this fact allows one to set up an asymptotic treatment in inverse powers of Q. This treatment in turn leads to the formulation of the problem as an eigenvalue problem for the Nusselt number (and oscillation frequency in the case of overstable convection). In the overstable regime the solutions of this problem revealed two types of dynamical behaviour in the nonlinear regime. The first regime, called here the 'vertical' regime, is characterized by a monotonically increasing Nusselt number and a broad isothermal interior flanked by narrow thermal boundary layers at the top and bottom, at least for sufficiently supercritical Rayleigh numbers. This regime is found in both steady and oscillatory convection unless the inclination of the field to the vertical is too large.

For large inclinations we have found in the overstable regime an unexpected hysteretic transition to a new regime which we have called the 'horizontal' regime. In this regime the Nusselt number no longer increases with the applied Rayleigh number, and may even decrease. This state is characterized by a modest isothermal core flanked by broad stagnant magnetic boundary layers at the top and bottom. We have argued that in this regime the energy input is stored in the deformation of the magnetic field instead of being transported convectively and supported this conclusion by additional diagnostics. We anticipate that in the full equations the Nusselt number in the horizontal regime will eventually start to increase with the applied Rayleigh number, probably as $Ra^{1/3}$, instead of the $Ra \ln Ra$ behaviour characteristic of the vertical regime in the scaling explored here.

This novel convection regime persists for all $O(Q^{1/4})$ wavenumbers, and does not depend on fixing $k_{0\perp}$, as in most of the results reported in this paper, or fixing k_0, although in the latter case no amount of tilt will produce this regime if the Rayleigh number is insufficiently large. We believe therefore that the 'horizontal' convection regime is a general feature of strongly nonlinear convection in oblique magnetic fields that is independent of the specific scaling used here to demonstrate its presence. Our results point to the important role played by the convection wavenumber and hence to the importance of wavenumber selection in the nonlinear regime. A possible approach to determining self-consistently the preferred wavenumber in this regime is described by Murphy & Lopez (1987).

The results of this paper are obtained using an asymptotically exact set of equations valid in the limit of large Q. As mentioned in the introduction these equations are closely related to the mean-field Ansatz, provided that the Laplacian operator is consistently replaced by D^2, the Rayleigh number is properly related to Q and the notion of averaging is extended, for time-periodic states, to averaging over time as well. The asymptotic procedure used here establishes that under these additional conditions the mean-field Ansatz provides an approximation to the correct behaviour that becomes more and more accurate as Q becomes larger and larger. Although this approach does not permit us to study the general stability properties of the solutions we used, wherever possible, standard exchange of stability arguments to infer the stability of the various solution branches. Elsewhere we have argued (Julien *et al.* 1999*a*) that we expect the strong magnetic field to keep any unstable solutions close to the inclined solutions we have constructed and as a result expect our solutions to provide a good description of the mean state of the system even if that

is turbulent. Julien & Knobloch (1998) provide evidence that this is so for strongly nonlinear convection on an f-plane. In a future paper we will report on the results of direct numerical simulations of two-dimensional magnetoconvection in a tilted field, focusing on the horizontal field regime identified here for comparison with the asymptotic theory.

It is tempting to speculate about the possible role of the fully nonlinear solutions discovered here in the structure of a sunspot. Sunspots consist of a dark central region, the umbra, surrounded by a non-axisymmetric filamentary penumbra. The penumbra is characterized by radial striations of alternating bright and dark filaments. The reason for the sudden transition between the umbra and the penumbra is poorly understood – but the nonlinear results discussed above suggest a possible mechanism. Observations have shown (e.g. Title *et al.* 1992) that the magnetic field strength does not change significantly across the spot, but that the tilt angle does vary significantly. In the sunspot umbra the tilt of the magnetic field increases with the distance from the centre, reaching 45° at the umbra–penumbra boundary (Thomas & Weiss 1992) and 70° at the edge of the spot.

Danielson (1961) in his study of tilted magnetoconvection speculated that a gradual change in tilt angle would lead to a change in the nature of convection from three-dimensional to two-dimensional but did not explain why the transition should be so abrupt. The results described in this paper suggest a possible scenario. For small tilt angles the system shows little preference between parallel and perpendicular rolls and the convection is expected to be fully three-dimensional. (For vertical magnetic fields the results of Clune & Knobloch (1993) indicate that, in the weakly nonlinear regime, three-dimensional structures are preferred at large Q if the onset of convection is oscillatory.) Moreover, both parallel and perpendicular rolls remain on the vertical field branch as the tilt angle is increased (at fixed supercritical Ra) and both transport energy efficiently. We have seen, however, that there is a critical tilt angle ϑ_c at which there is a saddle-node bifurcation beyond which the system settles onto the horizontal field branch. Although such a saddle-node bifurcation is present for both perpendicular and parallel rolls it is encountered first for the perpendicular rolls as ϑ (or, equivalently, the radial distance from the spot centre) increases. As described above, the convection on the horizontal field branch is very inefficient and for $\vartheta > \vartheta_c$ the Nusselt number drops to small values. This argument suggests that for $\vartheta > \vartheta_c$ heat will be transported only by parallel (i.e. radial) rolls which continue to be efficient transporters of heat; we suppose these to be in the form of standing waves.

This argument provides a natural and promising explanation for the observed sharp transition from three-dimensional to two-dimensional radial structures observed in sunspots, as discussed further elsewhere (Julien *et al.* 1999*b*), and has much in common with the sunspot model put forward by Rucklidge *et al.* (1995). In particular both explanations rely on saddle-node bifurcations present in a fully nonlinear model to explain the abrupt nature of the umbra–penumbra transition. Since the theory presented here is an asymptotic one valid only in the limit of large Q it is important to verify that the phenomena described here persist for finite Q in direct numerical simulations. We believe that our results provide an excellent motivation for pursuing such calculations.

This work was supported by NASA under SR&T grant NAG5-4918 (KJ), the Department of Energy under Grant No. DE-FG03-95ER-25251 (EK) and NASA under SPTP grant NAG5-2256 (SMT). The authors would like to thank Alastair Rucklidge and Nigel Weiss for helpful discussions.

Appendix. The nonlinear terms in the streamfunction representation

In the streamfunction representation the nonlinear terms appearing in equations (2.9)–(2.13),

$$N_\phi(\phi,\psi) \equiv (\boldsymbol{\omega}\cdot\nabla)w - (\boldsymbol{u}\cdot\nabla)\omega_3, \tag{A 1}$$

$$M_\phi(A,B) \equiv (\boldsymbol{j}\cdot\nabla)b_3 - (\boldsymbol{b}\cdot\nabla)j_3, \tag{A 2}$$

$$N_\psi(\phi,\psi) \equiv \hat{\boldsymbol{z}}\cdot\nabla\times\nabla\times(\boldsymbol{\omega}\times\boldsymbol{u}), \tag{A 3}$$

$$M_\psi(A,B) \equiv \hat{\boldsymbol{z}}\cdot\nabla\times\nabla\times(\boldsymbol{j}\times\boldsymbol{b}), \tag{A 4}$$

$$N_T(\phi,\psi,T) \equiv \boldsymbol{u}\cdot\nabla T, \tag{A 5}$$

$$M_A(\phi,\psi,A,B) \equiv \hat{\boldsymbol{z}}\cdot\nabla\times\nabla\times(\boldsymbol{u}\times\boldsymbol{b}), \tag{A 6}$$

$$M_B(\phi,\psi,A,B) \equiv (\boldsymbol{b}\cdot\nabla)w - (\boldsymbol{u}\cdot\nabla)b_3, \tag{A 7}$$

take the form

$$\begin{aligned} N_\phi = {} & -\mathrm{J}[\phi,\nabla_\perp^2\phi] - \mathrm{J}[\nabla^2\psi,\nabla_\perp^2\psi] + \nabla_\perp(\nabla_\perp^2\phi)\cdot\nabla_\perp(\partial_z\psi) \\ & -\nabla_\perp(\partial_z\phi)\cdot\nabla_\perp(\nabla_\perp^2\psi) - \nabla_\perp^2\psi\nabla_\perp^2(\partial_z\phi) + \nabla_\perp^2\phi\nabla_\perp^2(\partial_z\psi), \end{aligned} \tag{A 8}$$

$$\begin{aligned} M_\phi = {} & -\mathrm{J}[A,\nabla_\perp^2 A] - \mathrm{J}[\nabla^2 B,\nabla_\perp^2 B] + \nabla_\perp(\nabla_\perp^2 A)\cdot\nabla_\perp(\partial_z B) \\ & -\nabla_\perp(\partial_z A)\cdot\nabla_\perp(\nabla_\perp^2 B) - \nabla_\perp^2 B\nabla_\perp^2(\partial_z A) + \nabla_\perp^2 A\nabla_\perp^2(\partial_z B), \end{aligned} \tag{A 9}$$

$$\begin{aligned} N_\psi = {} & -\nabla^2\left\{\mathrm{J}[\phi,\nabla^2\psi] + \mathrm{J}[\partial_z\phi,\partial_z\psi] - \nabla_\perp\phi\cdot\nabla_\perp(\partial_z\phi) - \nabla_\perp(\partial_z\psi)\cdot\nabla_\perp(\nabla^2\psi)\right\} \\ & -\partial_z\{\mathrm{J}[\partial_z\psi,\nabla^2\phi] - \mathrm{J}[\phi,\nabla^2\partial_z\psi] - 2\mathrm{J}[\partial_z\phi,\nabla^2\psi] + \nabla_\perp\phi\cdot\nabla_\perp(\nabla^2\phi) \\ & +\nabla_\perp(\partial_z\psi)\cdot\nabla_\perp(\nabla^2\partial_z\psi) + \nabla_\perp^2\psi\nabla^2(\nabla_\perp^2\psi) + |\nabla_\perp(\partial_z\phi)|^2 \\ & +|\nabla_\perp(\nabla^2\psi)|^2 + (\nabla_\perp^2\phi)^2\}, \end{aligned} \tag{A 10}$$

$$\begin{aligned} M_\psi = {} & -\nabla^2\{\mathrm{J}[A,\nabla^2 B] + \mathrm{J}[\partial_z A,\partial_z B] - \nabla_\perp A\cdot\nabla_\perp(\partial_z A) - \nabla_\perp(\partial_z B)\cdot\nabla_\perp(\nabla^2 B)\} \\ & -\partial_z\{\mathrm{J}[\partial_z B,\nabla^2 A] - \mathrm{J}[A,\nabla^2\partial_z B] - 2\mathrm{J}[\partial_z A,\nabla^2 B] + \nabla_\perp A\cdot\nabla_\perp(\nabla^2 A) \\ & +\nabla_\perp(\partial_z B)\cdot\nabla_\perp(\nabla^2\partial_z B) + \nabla_\perp^2 B\nabla^2(\nabla_\perp^2 B) + |\nabla_\perp(\partial_z A)|^2 \\ & +|\nabla_\perp(\nabla^2 B)|^2 + (\nabla_\perp^2 A)^2\}, \end{aligned} \tag{A 11}$$

$$N_T = -\mathrm{J}[\phi,T] + \nabla_\perp\partial_z\psi\cdot\nabla_\perp T - \nabla_\perp^2\psi\partial_z T, \tag{A 12}$$

$$\begin{aligned} M_A = {} & \nabla^2\{\mathrm{J}[A,\phi] + \mathrm{J}[\partial_z B,\partial_z\psi] + \nabla_\perp A\cdot\nabla_\perp(\partial_z\psi) - \nabla_\perp\phi\cdot\nabla_\perp(\partial_z B)\} \\ & +\partial_z\{\mathrm{J}[\phi,\partial_z A] - \mathrm{J}[A,\partial_z\phi] + \mathrm{J}[\partial_z\psi,\nabla^2 B] - \mathrm{J}[\partial_z B,\nabla^2\psi] + \nabla_\perp^2 B\nabla_\perp^2\phi - \nabla_\perp^2\psi\nabla_\perp^2 A \\ & +\nabla_\perp\phi\cdot\nabla_\perp(\nabla^2 B) - \nabla_\perp A\cdot\nabla_\perp(\nabla^2\psi) \\ & -\nabla_\perp(\partial_z\psi)\cdot\nabla_\perp(\partial_z A) + \nabla_\perp(\partial_z B)\cdot\nabla_\perp(\partial_z\phi)\}, \end{aligned} \tag{A 13}$$

$$\begin{aligned} M_B = {} & -\mathrm{J}[\phi,\nabla_\perp^2 B] + \mathrm{J}[A,\nabla_\perp^2\psi] + \nabla_\perp(\partial_z\psi)\cdot\nabla_\perp(\nabla_\perp^2 B) \\ & -\nabla_\perp(\partial_z B)\cdot\nabla_\perp(\nabla_\perp^2\psi) - \nabla_\perp^2\psi\ \nabla_\perp^2(\partial_z B) + \nabla_\perp^2 B\ \nabla_\perp^2(\partial_z\psi), \end{aligned} \tag{A 14}$$

with the horizontal Jacobian operator $\mathrm{J}[\cdot,\cdot] \equiv \partial_x\cdot\partial_y\cdot - \partial_y\cdot\partial_x\cdot$.

REFERENCES

Arter, W. 1983 Nonlinear convection in an imposed horizontal magnetic field. *Geophys. Astrophys. Fluid Dyn.* **25**, 259–292.

Babin, A., Mahalov, A. & Nicolaenko, B. 1994 Long-time averaged Euler and Navier-Stokes equations for rotating fluids. In *Structure and Dynamics of Nonlinear Waves in Fluids* (ed. K. Kirchgässner & A. Mielke), pp. 145–157. World Scientific.

Bassom, A. P. & Zhang, K. 1994 Strongly nonlinear convection cells in a rapidly rotating fluid layer. *Geophys. Astrophys. Fluid Dyn.* **76**, 223–238.

Blennerhassett, P. J. & Bassom, A. P. 1994 Nonlinear high-wavenumber Bénard convection. *IMA J. Appl. Maths* **52**, 51–77.

Brownjohn, D. P., Hurlburt, N. E., Proctor, M. R. E. & Weiss, N. O. 1995 Nonlinear compressible magnetoconvection. Part 3. Travelling waves in a horizontal field. *J. Fluid Mech.* **300**, 287–309.

Cash, J. R. & Singhal, A. 1982 High order method for the numerical solution of two-point boundary value problems. *B.I.T.* **22**, 184–199.

Cattaneo, F. & Hughes, D. W. 1988 The nonlinear breakup of a magnetic layer: instability to interchange modes. *J. Fluid Mech.* **196**, 323–344.

Chandrasekhar, S. 1961 *Hydrodynamic and Hydromagnetic Stability*. Oxford University Press.

Clune, T. & Knobloch, E. 1993 Pattern selection in three-dimensional magnetoconvection. *Physica* D **74**, 151–176.

Danielson, R. E. 1961 The structure of sunspot penumbras. II. Theoretical. *Astrophys. J.* **134**, 289–311.

Henrici, P. 1962 *Discrete Variable Methods in Ordinary Differential Equations*. Wiley and Sons.

Hughes, D. W. 1987 Finite amplitude solutions for interchange instabilities driven by magnetic buoyancy. *Geophys. Astrophys. Fluid Dyn.* **37**, 297–343.

Julien, K. & Knobloch, E. 1997 Fully nonlinear oscillatory convection in a rotating layer. *Phys. Fluids* **9**, 1906–1913.

Julien, K. & Knobloch, E. 1998 Strongly nonlinear convection cells in a rapidly rotating fluid layer: the tilted f-plane. *J. Fluid Mech.* **360**, 141–178.

Julien, K., Knobloch, E. & Tobias, S. M. 1999*a* Strongly nonlinear magnetoconvection in three dimensions. *Physica* D **128**, 105–129.

Julien, K., Knobloch, E. & Tobias, S. M. 1999*b* Highly supercritical convection in strong magnetic fields. In *The Fluid Dynamics of Geophysics and Astrophysics* (ed. Ferriz-Mas & M. Núñez). Gordon & Breach, to appear.

Knobloch, E. 1994 Bifurcations in rotating systems. In *Lectures on Solar and Planetary Dynamics* (ed. M. R. E. Proctor & A. D. Gilbert), pp. 331–372. Cambridge University Press.

Knobloch, E. & Merryfield, W. J. 1992 Enhancement of diffusive transport in oscillatory flows. *Astrophys. J.* **401**, 196–205.

Matthews, P. C. 1999 Asymptotic solutions for nonlinear magnetoconvection. *J. Fluid Mech.* **387**, 397–409.

Matthews, P. C., Hurlburt, N. E., Proctor, M. R. E. & Brownjohn, D. P. 1992 Compressible magnetoconvection in oblique fields: linearized theory and simple nonlinear models. *J. Fluid Mech.* **240**, 559–569.

Matthews, P. C., Proctor, M. R. E., Rucklidge, A. M. & Weiss, N. O. 1993 Pulsating waves in nonlinear magnetoconvection. *Phys. Lett.* A **183**, 69–75.

Murphy, J. O. & Lopez, J. M. 1987 Evolution of a horizontal scale for magnetoconvection. *Proc. ASA* **7**, 112–116.

Proctor, M. R. E. 1986 Columnar convection in double-diffusive systems. *Contemp. Maths* **56**, 267–276.

Rucklidge, A. M., Schmidt, H. U. & Weiss, N. O. 1995 The abrupt development of penumbrae in sunspots. *Mon. Not. R. Astron. Soc.* **273**, 491–498.

Silber, M., Riecke, H. & Kramer, L. 1992 Symmetry-breaking Hopf bifurcation in anisotropic systems. *Physica* D **61**, 260–278.

Thomas, J. H. & Weiss, N. O. 1992 The theory of sunspots. In *Sunspots: Theory and Observations* (ed. J. H. Thomas & N. O. Weiss), pp. 3–59. Kluwer.

Title, A. M., Frank, Z. A., Shine, R. A., Tarbell, T. D., Topka, K. P., Scharmer, G. & Schmidt,

W. 1992 High resolution observations of the magnetic and velocity field of simple sunspots. In *Sunspots: Theory and Observations* (ed. J. H. Thomas & N. O. Weiss), pp. 195–219. Kluwer.

Van der Borght, R. & Murphy, J. O. 1973 The combined effect of rotation and magnetic field on finite-amplitude thermal convection. *Austral J. Phys.* **26**, 617–643.

Veronis, G. 1959 Cellular convection with finite amplitude in a rotating fluid. *J. Fluid Mech.* **5**, 401–435.

Weiss, N. O. 1981*a* Convection in an imposed magnetic field. Part 1. The development of nonlinear convection. *J. Fluid Mech.* **108**, 247–272.

Weiss, N. O. 1981*b* Convection in an imposed magnetic field. Part 2. The dynamical regime. *J. Fluid Mech.* **108**, 273–289.

Weiss, N. O., Brownjohn, D. P., Hurlburt, N. E. & Proctor, M. R. E. 1990 Oscillatory convection in sunspot umbrae. *Mon. Not. R. Astron. Soc.* **245**, 434–452.

Weiss, N. O., Brownjohn, D. P., Matthews, P. C. & Proctor, M. R. E. 1996 Photospheric convection in strong magnetic fields. *Mon. Not. R. Astron. Soc.* **283**, 1153–1164.